AFFDL-TR-65-192
VOLUME II

AERODYNAMIC NOISE TESTS ON X-20 SCALE MODELS

VOLUME II. SUMMARY AND ANALYSIS REPORT

DAVID R. WILEY and MICHAEL G. SEIDL

THE BOEING COMPANY

TECHNICAL REPORT AFFDL-TR-65-192, VOL. II

NOVEMBER 1965

AIR FORCE FLIGHT DYNAMICS LABORATORY
RESEARCH AND TECHNOLOGY DIVISION
AIR FORCE SYSTEMS COMMAND
WRIGHT-PATTERSON AIR FORCE BASE, OHIO

NOTICES

When Government drawings, specifications, or other data are used for any purpose other than in connection with a definitely related Government procurement operation, the United States Government thereby incurs no responsibility nor any obligation whatsoever; and the fact that the Government may have formulated, furnished, or in any way supplied the said drawings, specifications, or other data, is not to be regarded by implication or otherwise as in any manner licensing the holder or any other person or corporation, or conveying any rights or permission to manufacture, use, or sell any patented invention that may in any way be related thereto.

Copies of this report should not be returned to the Research and Technology Division unless return is requred by security considerations, contractual obligations, or notice on a specific document.

200 - January 1966 - 24-477-773

AERODYNAMIC NOISE TESTS ON X-20 SCALE MODELS

VOLUME II. SUMMARY AND ANALYSIS REPORT

DAVID R. WILEY and MICHAEL G. SEIDL

FOREWORD

This research effort was performed by The Boeing Company, Aerospace Group, Seattle, Washington, for the Aero-Acoustics Branch, Vehicle Dynamics Division, Air Force Flight Dynamics Laboratory, Wright-Patterson Air Force Base, Ohio. It was performed under Reinstated Documentation Sub-Item No. 8-46 of Contract AF33(657)-7132 for the development of the X-20 or Dyna Soar. This was one of a number of technical developments of the X-20 program that appeared to merit completion for its own contribution to aerospace technology after the basic program was terminated. The research effort is part of a continuing effort to predict and control the aero-acoustic environment of flight vehicles and is part of the Research and Technology Division, Air Force Systems Command's exploratory development program. The work was directed under Project 1471, "Aero-Acoustic Problems," Task 147102,"Prediction and Control of Noise," with Mr. D. L. Smith as technical monitor.

This program was conducted from October 1964 to August 1965 by David R. Wiley and Michael G. Seidl, with technical assistance from other members of the Boeing Aero-Space Group's Acoustics organization, under the supervision of Kenneth J. Young. A Boeing Report No. D2-23966-2 has been assigned for internal control.

The manuscript of this report was released by the authors on 13 September 1965 for publication as an AFFDL Technical Report.

This technical report has been reviewed and is approved.

Walter J. Mykytow
WALTER J. MYKYTOW
Asst. for Research & Technology
Vehicle Dynamics Division

ABSTRACT

Summaries of fluctuating pressure data presented in Volume 1 for 1/15th-scale X-20 models are made and discussed. Particular emphasis is given to the high overall rms pressures measured aft of convex corners during transonic test conditions. Additional information relating to these pressures is presented in the form of pressure histories, peak-amplitude distributions, and power spectral densities. Fluctuating-pressure data and space correlation measurements for three closely spaced microphones are presented, illustrating the local nature of the high-level pressures. Analyses of trends for the maximum overall rms pressure levels for the X-20 tests and other wind-tunnel tests are made. Design charts are developed for predicting maximum levels aft of cone-cylinder transition sections as functions of transition angle and distance downstream of the transition shoulder. Recommendations are made regarding future aerodynamic noise experimental programs.

CONTENTS

ILLUSTRATIONS

ILLUSTRATIONS (Cont.)

TABLES

ABBREVIATIONS AND SYMBOLS

A	microphone designation for Ames wind tunnel test
B	microphone designation for Boeing wind tunnel test
C_p	$\frac{p_{local} - p_\infty}{q_\infty}$, pressure coefficient
M	Mach number
SPL	sound pressure level in db re 0.0002 microbar (overall, unless otherwise noted).
V_∞	free-stream velocity
d	diameter
f	frequency
p_{local}	local static pressure
$p_n(t)$	pressure at microphone n at time t
p_{rms}	$\left[\int_0^\infty \frac{\text{band level, (psi)}^2}{\text{bandwidth, (cps)}}\ df\right]^{1/2}$ overall pressure value computed graphically from measured data assuming the trend of level vs. frequency can be extrapolated outside of measured frequency range.
p_∞	free-stream static pressure
q_∞	free-stream dynamic pressure
x	distance aft of shoulder
α	angle of attack (positive when nose is up)
β	yaw angle (positive when nose is right as viewed from top)
δ^*	boundary layer displacement thickness

1.0 INTRODUCTION

Boundary-layer noise, which is generated by turbulent flow, has been investigated both theoretically and experimentally for the past decade. Methods have been developed for predicting sound spectra from given values of density, velocity, and boundary-layer displacement thickness. The methods, however, are applicable only to smoothly contoured vehicles and for conditions of attached flow with no shocks. Flight and wind-tunnel tests have shown that fluctuating pressures exist on localized areas of a vehicle during transonic flight that are many times greater than normal attached-boundary-layer noise pressures. These higher rms pressures are associated with fluctuating shocks and separated flow near vehicle contour changes or surface irregularities. Because of potential structural failures and equipment malfunctions, it is important to have methods available for predicting all forms of aerodynamically generated noise. Specifically, it is desirable to predict the sound spectra associated with various flight conditions and local vehicle geometry.

During the X-20 program, wind-tunnel tests were conducted on 1/15-scale models of the X-20 vehicle. The first test, conducted in Boeing wind tunnels, consisted of 480 test runs with the glider; the other test, in the 14-foot transonic wind tunnel at Ames Research Center, included 202 test runs with the glider as a payload on a Titan 624A booster. Test reports were released (Refs. 1 and 2) that give data from selected test conditions. (These references contain only the data; no analysis of trends is included.) A great range of additional test data existed, most of it still on magnetic tape, that could form the basis for a more general analysis of aerodynamic noise.

This program was undertaken to further reduce and analyze data from the above wind-tunnel tests. In selecting the test runs to be included in the study, transonic tunnel conditions and regions near vehicle contour changes were emphasized. Volume 1, the data report for this program, contains more than 3500 curves showing octave-band sound pressure level versus frequency. This document, Volume 2, is the summary and analysis report, and also contains the results of several types of data reduction not included in the first volume.

2.0 BACKGROUND

2.1 TYPES OF FLOW

Fluctuating forces of aerodynamic origin occur on the surface of a flight vehicle as a result of various flow conditions. The fluctuating forces of primary interest result from (1) the passage of turbulent eddies within the boundary layer, (2) recirculatory flow or vortices within separated flow or wake regions, (3) shock-wave/boundary-layer interaction, and (4) alternations from separated to attached flow. In addition to these wide-band, random pressures, discrete-frequency pressures produced by the Von Karman vortex-street phenomenon may occur downstream of sharp protuberances such as antennas. No such discrete frequencies were detected during X-20 model testing; as a result, this phenomenon is not discussed here.

At low-subsonic Mach numbers, the flow around the vehicle is attached, and the primary source of fluctuating pressure is the convected field of eddies formed by the scrubbing action of the flow against the vehicle skin. This type of pressure fluctuation, resulting from turbulent attached boundary layers, has been investigated by several experimenters. Surfaces used for the measurements have included wind-tunnel models, wind-tunnel walls, flat plates, pipes, glider wings, and other smoothly contoured flight-vehicle surfaces. Although considerable work is needed in collating the results of different investigators, it is believed that the results of these studies can be collapsed to a reasonable set of data on the basis of (1) a nondimensional Strouhal frequency parameter formed by the product of measured frequency with boundary-layer displacement thickness and the reciprocal of the eddy convection velocity, and (2) a pressure-level parameter such that the overall rms pressure is proportional to dynamic pressure. The overall rms pressure is taken to be nominally $0.006\ q_\infty$. The peak of the spectrum (constant-percentage-bandwidth plot) occurs at a Strouhal number ($f\ \delta^*/V_\infty$) of approximately 0.14. More recent investigations (Ref. 3) have indicated that a better scaling parameter for the pressure level is skin friction, τ_w, which is closely related to the state of the boundary layer.

At higher Mach numbers, the boundary layer separates from areas of the body where the flow passes sharp, convex corners such as boat-tail sections and cone-to-cylinder transition sections. For the cone-to-cylinder transitions of interest here, the flow is first compressed on the increasing cross section of the cone. It then expands, passing through an abrupt reduction in pressure at the corner, which strongly accelerates the flow to velocities greater than free-stream velocity. Progressing aft of the corner, the flow is decelerated toward free-stream conditions and the boundary layer moves into an adverse pressure gradient. Depending on the state of the boundary layer at the corner and the magnitude of the adverse pressure gradient, the boundary layer either remains attached or becomes separated, with possible reattachment further downstream. Within the separated zone, the positive pressure gradient causes flow in the direction opposite to the free stream.

A typical pressure distribution on a cone-cylinder model in separated flow is shown in Figure 1(a). The velocity profiles indicate the direction of the mean flow near the model. The reverse flow in the separated region interacts with the turbulent, separated boundary layer, causing recirculatory eddies within the region that result in unsteady pressures on the vehicle skin. The time-varying pressure arising from separated-flow turbulence is similar to the pressure from an attached boundary layer in that it has random amplitude variations symmetric about the mean pressure present; however, it is larger in overall magnitude and has greater low frequency content than would be predicted on the basis of dynamic pressure and boundary-layer displacement thickness. Separated flows can cover large areas of the vehicle, and, with low back-flow velocities, significantly large areas of positively correlated pressures could result.

As the Mach number is further increased, the flow around the corner becomes supersonic and significantly compressible, so that the flow is attached for some distance downstream of the shoulder where the supersonic zone is terminated by a near-normal shock that strongly interacts with the boundary layer. This flow condition is sketched in Figure 1(b). Within the attached portion of the flow upstream of the shock wave, the fluctuating pressure observed should be of the same level and frequency as predicted from normalized experimental data based on δ^*, V_∞, and q_∞ or τ_w. Downstream of the shock where the severe adverse pressure gradient of the shock has caused the boundary layer to separate, fluctuating pressures, characteristic of separated flow, result. The subsonic boundary layer allows the higher pressure downstream of the shock wave to feed forward under the shock; this in turn increases the pressure gradient at that point and tends to move the boundary-layer separation point upstream. The balance between the initial flow conditions that position the shock and the tendency of the shock to move forward is unstable; this causes the shock to move randomly about a small region of the vehicle so that the flow in this region alternates randomly between attached and separated conditions. The resulting pressure is first a fluctuating pressure characteristic of the attached-flow condition, and, alternately, a fluctuating pressure characteristic of separated flow. The latter pressures are of a relatively higher rms value. In addition to the different rms fluctuating pressure levels, a different mean pressure is associated with each flow state, which causes the pressure felt by the skin as a function of time to appear as a rectangular wave train of fixed peak-to-peak amplitude (Δp in Figure 1(b)), but randomly varying pulse width. This is in addition to the superimposed random amplitude noise that is characteristic of the particular flow state. Areas of negative correlation are produced by the opposite directions of the pressure change fore and aft of the shock, and a large time-varying couple about that point is imposed on the vehicle surface.

Reported static pressure distributions for cone-cylinder models indicate that peak-to-peak pressures as high as 60 percent of q_∞ may result from this flow instability (Ref. 4). Data reported in Reference 4 indicate that the back pressure behind the shock can move the shock forward to the shoulder, separating the flow at the shoulder. This is followed by reattachment of the flow and shock in cyclical

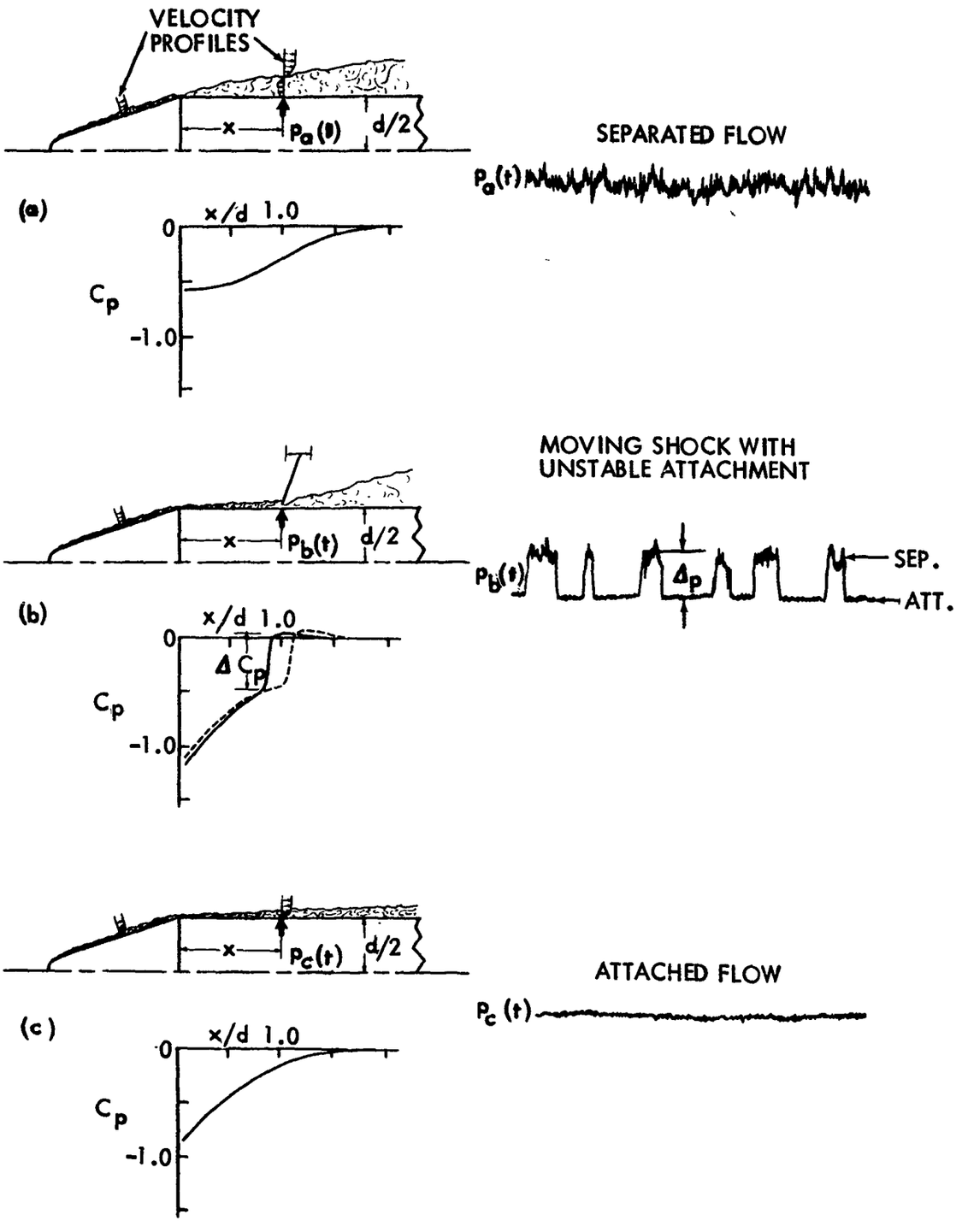

Figure 1: Sketch of Flow and Pressures on a Cone-Cylinder

fashion so that a fluctuating pressure between the two flow conditions would be imposed over a relatively large area of the vehicle. Measurements on the X-20 model and data reported in the literature, however, indicate that the highest rms pressures resulting from this flow instability are felt at a particular time only over a small area of the vehicle. Data and measurements also indicate that, with increasing Mach number, this rms pressure is reduced as the shock moves rearward on the vehicle, and that its interaction with the boundary layer is less pronounced. As the shock moves downstream of the shoulder, the pressure resulting from this interaction is expected to progress continuously from the predominantly low-frequency, high-level spectra imposed close to the shoulder to the low-level, high-frequency spectra characteristic of the undisturbed boundary layer.

At still higher Mach numbers, the shock moves aft of the vehicle, the boundary layer is attached over the entire region aft of the corner, and pressures are characteristic of attached-boundary-layer-flow noise. This flow condition is sketched in Figure 1(c).

Portions of the X-20 model not located near abrupt vehicle contour changes are expected to have an attached boundary layer throughout the transonic range. The overall rms pressure experienced should be approximately $0.006\ q_\infty$, with the frequency at which the noise spectrum reaches a peak, increasing in proportion to free-stream velocity.

Areas of the X-20 model aft of convex contour changes experience local flow accelerations. As the Mach number increases through the transonic range, these areas are expected to experience pressures characteristic of the different types of flow: (1) separated flow (p_{rms}/q_∞ on the order of 0.05), (2) shock/boundary-layer interaction ($p_{rms}/q_\infty > 0.1$), (3) supersonic attached flow ($p_{rms}/q_\infty \approx 0.006$). These areas are the top of the pilot's canopy and downstream of the transition section between the X-20 and its booster. Data obtained with microphones in these areas are emphasized in this report. At supersonic free-stream conditions, the attached boundary layers over the entire X-20 model are expected to produce overall rms pressures of less than $0.01\ q_\infty$, with the spectrum peaking at high frequencies. Analysis of supersonic data is not presented in this volume, but the data presented in Volume 1 indicate levels of this general magnitude.

2.2 SCALING

The scaling philosophy adopted in this study is as follows. A true geometric scale model with flow characteristics similar to those of a full-scale vehicle has the same overall rms pressure fluctuations at geometrically similar locations, but when applied to the full-scale vehicle spectrum, presented in constant-percentage-bandwidth form, undergoes a frequency shift inversely proportional to the scale factor. (This statement is based on dimensional analysis (Ref. 5), experimental data for acoustic models of jet flows (Ref. 6), and flows with attached boundary layers (Ref. 7).) For the model flow to be similar to full-scale flow, dimensional analysis indicates that Mach number and Reynolds number must be identical, but

this is not feasible for wind tunnels using air for the flow medium. The assumption that must be made, then, is that approximately similar flow results if Mach number and dynamic pressures are identical and if the Reynolds number for the model test is sufficiently high.

A summary of experimental and theoretical results relating transonic buffet pressure from models to full scale has been made by Rainey (Ref. 8). The conclusion reached is that it is reasonable to expect (1) that transonic buffet pressures are dimensionally well-behaved, and (2) that frequency scaling by the inverse-scale relationship is valid. In the current analysis, some additional data are presented that tend to strengthen the argument for scaling. It is recognized, however, that transonic data from a controlled set of models covering a wide scale range are required to fully validate the present scaling approach.

Based on the scaling considerations outlined above, the overall sound pressure levels presented in this report (both Volumes 1 and 2) are expected to be the same as those for a similar full-scale vehicle operating in a flow with identical Mach number and dynamic pressure, except that all octave band data for the model would be shifted downward in frequency by a factor of 15, the reciprocal of scale factor, to apply to the full-scale vehicle. To be strictly correct, the full-scale pressures predicted would be those that would be measured with full-scale transducers 15 times the effective diameter of the scale-model transducers, and would represent the pressure averaged over the active surface of the transducer.

2.3 DATA PRESENTATION FORM

In this report, the aerodynamic fluctuating pressure data are presented primarily in the form of sound pressure level (db) in constant-percentage frequency bands (e.g., octave) versus frequency, with each band level plotted at the center frequency of the band on a logarithmic scale; this is a common form for presenting acoustic data. Two other methods for presenting aerodynamic noise data are in common usage. These methods are (1) spectral density (psi^2/cps) versus frequency on linear scales, and (2) spectral density versus frequency on logarithmic scales. These three methods of presentation are compared in Figure 2 with data from Microphone Location A-33, both for the data measured on the 1/15-scale X-20 model and for the inferred pressure spectrum of a full-scale model.

In Figure 2(a), the plotting form for spectral density versus frequency with both scales linear makes the data from the two model sizes appear quite different, both in level and in spectrum shape. In this form, it is difficult to determine if the data for the two model sizes are compatible. Neither the overall level nor the frequency and level for the spectrum peak are obvious from either curve, and values at low and high frequencies are difficult to read because of the slopes of the curves that result from the great range of level and frequency necessary to plot aerodynamic fluctuating pressure data.

The logarithmic plot (Figure 2(b)) of these same data allows the spectral density to be read easily throughout the frequency range. The relative magnitude of the

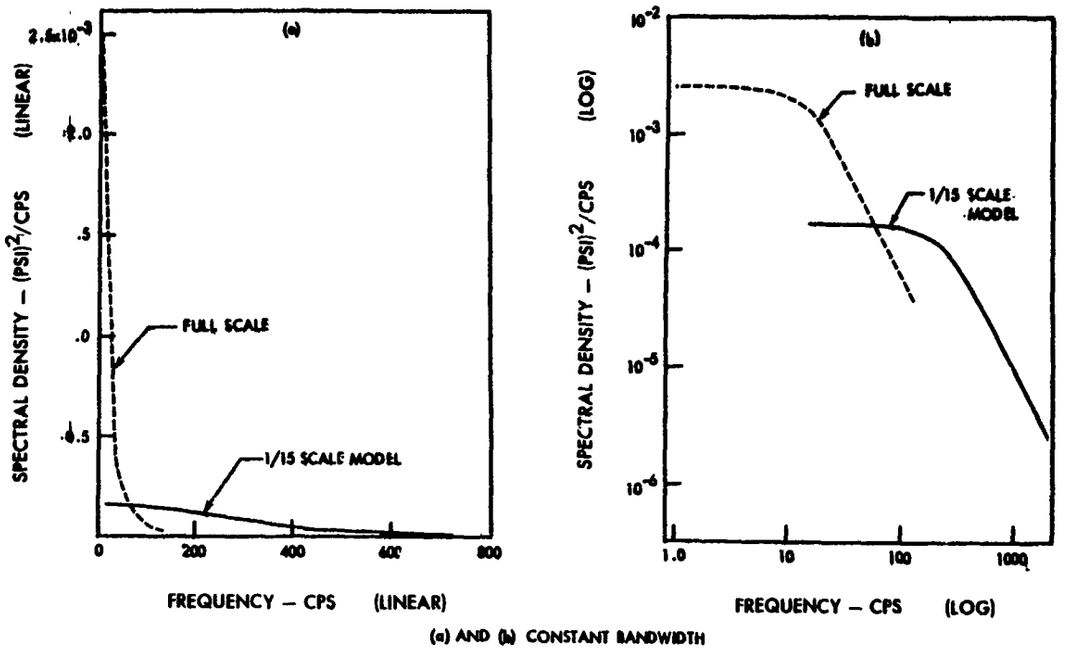

(a) AND (b) CONSTANT BANDWIDTH

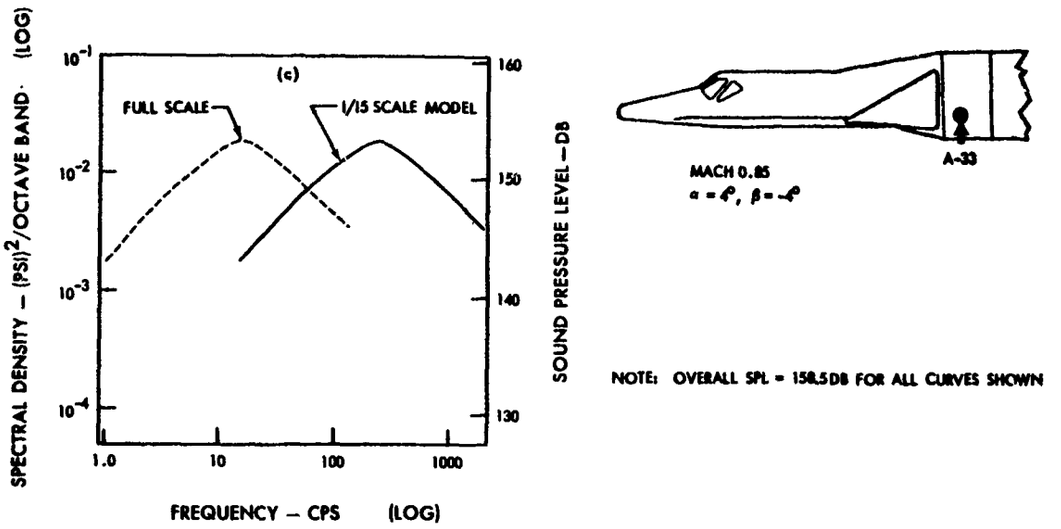

(c) CONSTANT PERCENTAGE BANDWIDTH

Figure 2: Comparison of Three Common Spectrum Presentations

(CURVES SHOWN ARE FOR 1/15 SCALE AND INFERRED VALUES FOR FULL SCALE.)

overall levels for the 1/15-scale model and the full-scale model is not apparent without close examination of the data, however, even when the overall levels are identical, as for the curves shown. To superpose the two curves, and thereby demonstrate that the data are related through the scale factor, it is necessary to shift the model data downward in frequency and upward in level, both shifts by a factor of 15. The actual frequency of the peak of the spectrum for this type of plot occurs at the knee of the curve.

In Figure 2(c) the data are presented in the form of mean-squared pressure per octave versus frequency, with logarithmic scales. The use of narrow bandwidths (e.g., 1/9th octave) is necessary to verify experimentally that discrete frequencies are not present in a particular noise sample. Full octave bandwidths, however, appear to be adequate for the definition of the "white" noise pressures resulting from flow noise. In the constant-percentage-bandwidth form, the reduced frequency scaling relationship for the two models is most readily apparent. This data presentation allows the relative magnitude of the overall levels and the magnitude of the frequency shift to be recognized immediately. Data from a variety of model sizes can be compared or normalized to full scale by a simple frequency shift, and no change in level is necessary. Since the spectrum peak is readily apparent, scaling relationships are detected easily. The equivalent decibel scale is shown to the right of Figure 2(c).

The conversion of measured band sound pressure levels (SPL_{Band}) in db re 0.0002 dyne/cm^2 to power spectral density, (psi)^2/cps, values is done in the following manner:

$$PSD = \text{antilog}\left\{\frac{SPL_{Band} - 170.8 - 10 \log\left(\frac{\Delta f,\ cps}{1\ cps}\right)}{10}\right\}$$

where 170.8 is the sound pressure level equivalent for 1.0 psi, and Δf is the bandwidth used. For N percentage bandwidth, $\Delta f = Nf_c/100$, where f_c is the center frequency (geometric mean) of the band. (N is 70.7 for an octave bandwidth.)

3.0 MODEL DESCRIPTION

For the Boeing transonic and supersonic tunnel tests, a 0.066-scale model of the X-20 glider was strut-sting mounted with 19 Statham pressure transducers installed to measure the fluctuating pressure on the model glider.

Two general model configurations were used throughout the Boeing tunnel tests:

1) Glider without transition section (Figure 3);

2) Glider with transition section (Figure 4).

Detailed locations of all glider pressure transducers used during the Boeing tunnel tests are shown in Figure 5.

In the Ames transonic tunnel tests, a 0.067-scale model configuration of an X-20 glider as a payload on a Titan 624A booster was used. Figure 6 shows the model mounted in the wind tunnel. The locations of pressure transducers used to measure aerodynamic noise on the model can be seen in Figure 7. (While 28 transducers were used in the test, only the 18 transducers selected for the present study are shown in Figure 7.)

The Ames model configuration included the X-20 heat shield over the forward portion of the canopy, whereas the Boeing model did not. This gives rise to different transition angles (θ) for the canopy region of the two models, the angle being 28 degrees for the Ames model and 36 degrees for the Boeing model.

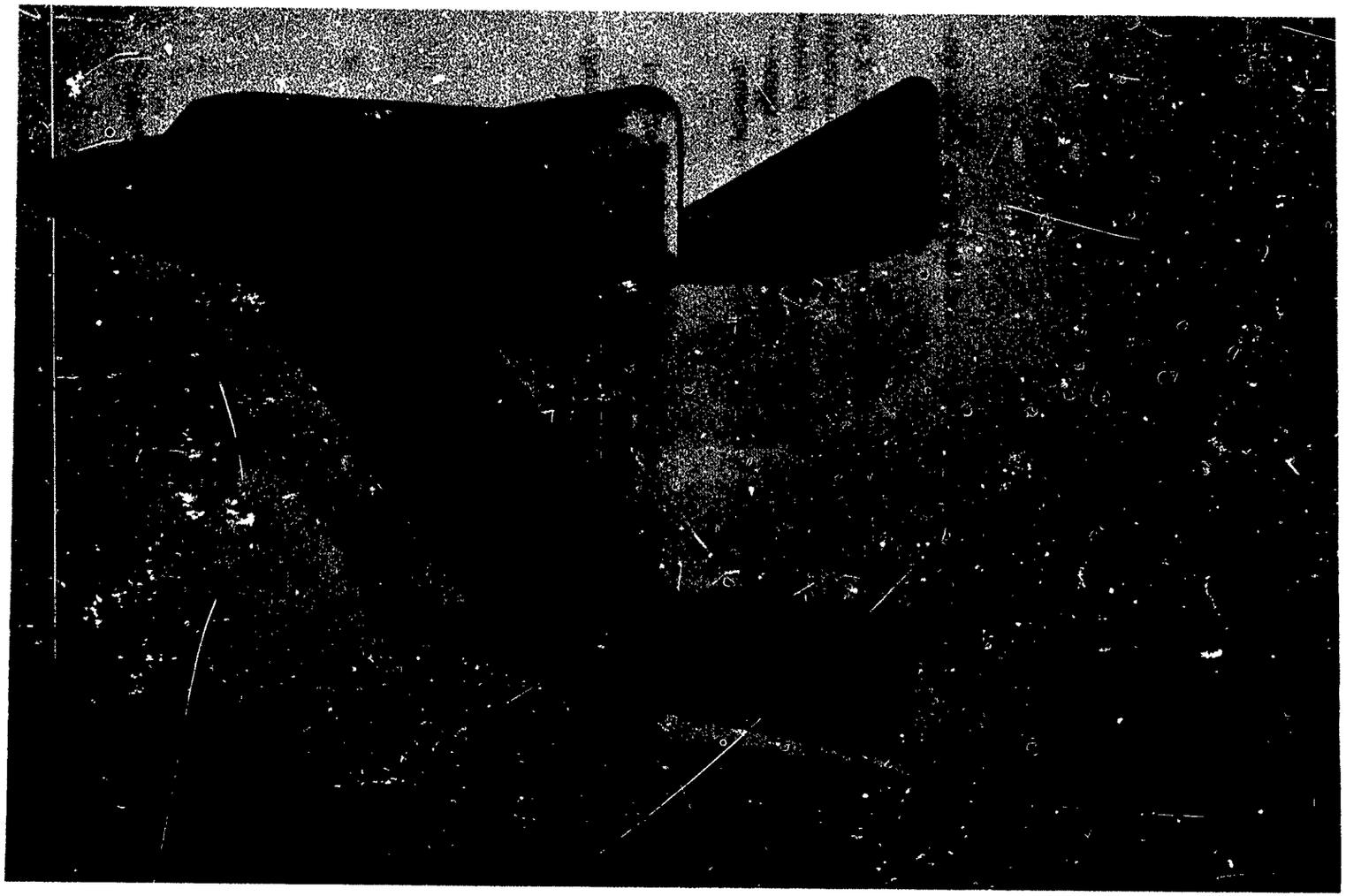

Figure 3 : Model Glider Without Transition Section (Boeing Tunnel Tests)

Figure 4 : Model Glider With Transition Section (Boeing Tunnel Tests)

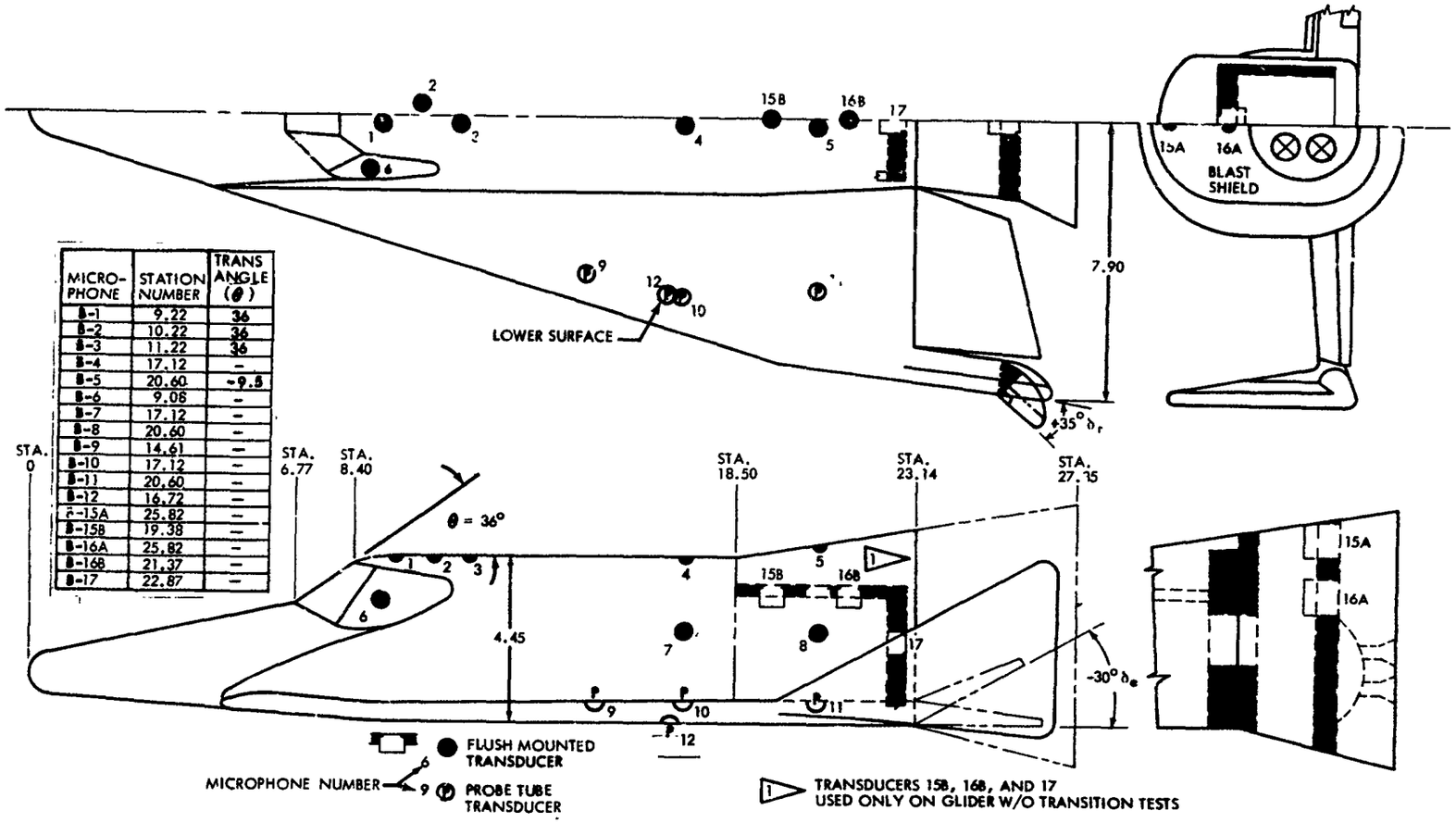

Figure 5 : Glider Pressure Transducer Locations (Boeing Tunnel Tests)

Figure 6 : Glider/Booster Model in Wind Tunnel (Ames Tests)

MICRO-PHONE	STATION NUMBER	TRANSITION ANGLE (θ-DEG)
A-2	10.70	28
A-3	20.45	-9.5
A-8	27.75	-
A-12	26.85	-
A-18	23.05	-8.5
A-20	25.80	-
A-21	26.90	-
A-26	29.50	8
A-27	29.50	26
A-28	29.50	21.5
A-29	29.50	16
A-30	31.05	8
A-31	31.05	17
A-32	31.05	26
A-33	31.05	21.5
A-34	31.05	16
A-35	31.05	16
A-36	34.10	26

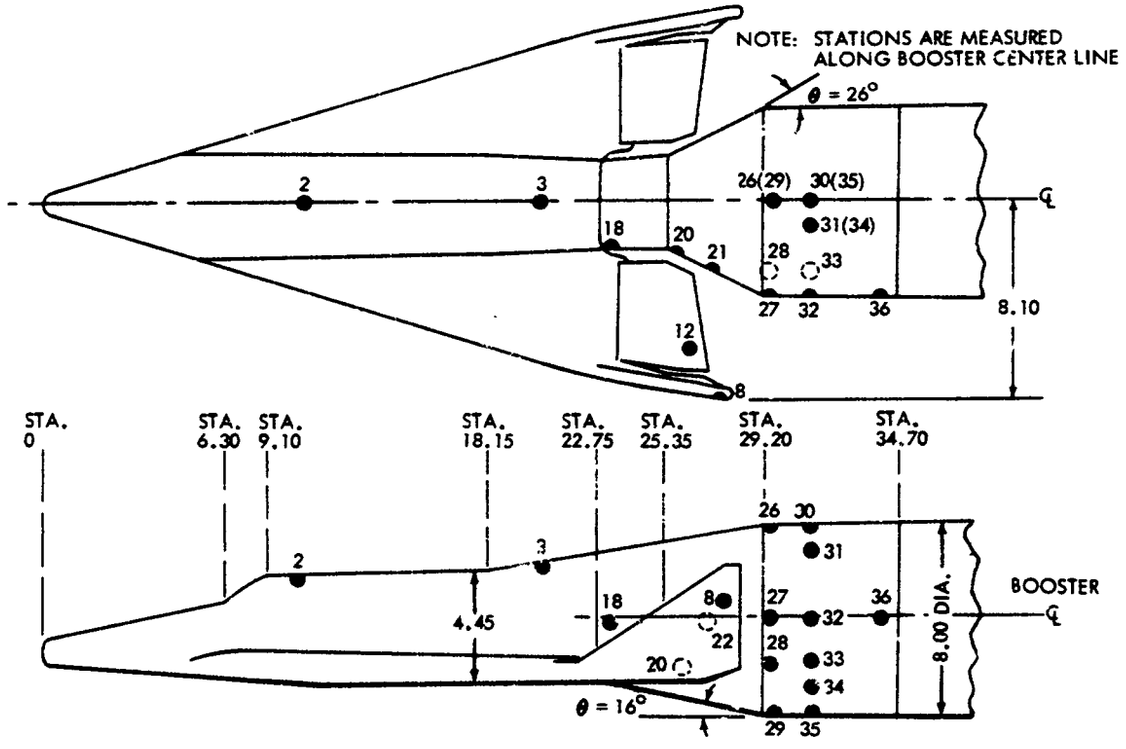

Figure 7: Glider/Booster Pressure Transducer Locations (Ames Tests)

4.0 INSTRUMENTATION

The instrumentation and calibration procedures used in the wind tunnel tests are described in Volume I. A few pertinent excerpts are given below.

For the Boeing tunnel tests, the Statham PA 208-TC pressure transducer was used to measure fluctuating pressures on the model glider. These transducers were rated to operate over a pressure range of 0 to 15 psi, and the transducer systems were capable of measurements over the frequency range of 0 to 5000 cps. Diaphragm diameter for these transducers was 0.50 inch. As indicated in Figure 5, probe tubes were used in the wing locations. The inner diameter of these tubes was 0.04 inch. Data were recorded using an Ampex FR-1100 tape recorder.

The pressure transducers used in the Ames tunnel tests were designed and fabricated by members of the Ames Research Center staff. They were a bonded strain-gage type, each consisting of two active elements, with an external bridge mounted near the active arms. On the model installation, the transducers were mounted with their 0.25-inch-diameter diaphragms flush with the model surface. Original recording of the data was accomplished using a Honeywell Model LAR 7400 tape recorder.

4.1 DATA REDUCTION

To obtain octave band sound pressure level readings from the magnetic tape, a Bruel and Kjaer system consisting of the Model 2112 spectrometer, 1620 extension filter, and 2305 graphic level recorder was used. The reference level was obtained from a calibration tone of known level on the tape.

The frequency response of the elements used in making the high-speed oscillograms shown in this report was within plus or minus 0.5 db from 0 to 3000 cycles per second.

For power spectral density measurements, the key instruments in the system were a Technical Products Company Model TP-627 analyzer, a TP-626 oscillator, and a TP-633 power integrator. Filter bandwidths used in the analyzer were 5 cps for the frequency range of 10 to 250 cps, 20 cps for the 250- to 1000-cps range, and 50 cps for frequencies greater than 1000 cps. The data sample length and scan period were 12 to 15 seconds; the integration time was 4 seconds.

Peak amplitude distribution measurements were made with a system using a Tektronix Model 545 oscilloscope as the trigger element. A timer of good repeatability operated a mercury relay to gate the noise sample. The voltage level corresponding to a particular peak-to-rms ratio for the noise sample was set on the oscilloscope, and the output pulse obtained from the oscilloscope for each trace triggering was counted on an electronic counter. The rms value of the narrow-band-limited noise sample was measured with a Ballentine Model 320

rms voltmeter. Care was taken to ensure that the sweep time on the oscilloscope was less than the period corresponding to the highest frequency component in the noise sample being measured, and that all amplifiers in the system had adequate peak-handling capabilities.

4.2 WIND-TUNNEL PARAMETERS

Nominal test section parameters for the wind tunnels are given in Tables 1, 2, and 3.

Table 1

Nominal Test Section Parameters (Boeing Transonic Tunnel)

MACH NUMBER	STATIC PRESSURE (PSFA)	DYNAMIC PRESSURE (PSFA)	TOTAL TEMP (°R)	REYNOLDS NUMBER/FT (10^6)
0.5	1780	315	566	2.86
0.6	1660	418	577	3.19
0.7	1530	523	583	3.48
0.8	1390	620	580	3.76
0.85	1310	667	582	3.85
0.9	1240	709	586	3.91
0.95	1180	746	593	3.92
1.0	1110	782	597	3.95
1.1	982	839	607	3.94

Table 2

Nominal Test Section Parameters (Boeing Supersonic Tunnel)

MACH NUMBER	TOTAL PRESSURE (PSFA)	STATIC PRESSURE (PSFA)	DYNAMIC PRESSURE (PSFA)	TOTAL TEMP (°R)	REYNOLDS NUMBER/FT (10^6)
1.5	2840	763	1200	510	6.5
2.0	3885	504	1400	510	7.5
2.5	5760	345	1500	510	8.8
3.0	8640	236	1500	510	10.0
3.5	12960	169	1450	515	11.8

Table 3

Nominal Test Section Parameters (Ames Transonic Tunnel)

M	TOTAL PRESSURE (PSFA)	STATIC PRESSURE (PSFA)	DYNAMIC PRESSURE (PSFA)	REYNOLDS NUMBER PER FT. (10^6)	TOTAL TEMPERATURE (^oR)	STATIC TEMPERATURE (^oR)	VELOCITY (FPS)
0.60	2100	1653	415.0	3.37	546.8	510.2	663
0.65	↓	1583	467.6	3.31	581.4	536.2	737
0.70		1518	520.7	3.65	558.9	509.0	787
0.725		1479	545.6	3.41	598.1	541.1	878
0.75		1456	566.3	3.73	565.5	509.3	824
0.8		1381	618.8	3.8	574.1	508.9	885
0.825		1353	635.8	3.83	573.1	504.4	909
0.85		1314	662.7	3.89	575.8	503.3	933
0.86		1297	671.8	3.83	584.5	509.1	951
0.875		1272	683.6	3.87	582.2	504.7	965
0.88		1269	688.3	3.86	585.7	507.1	971
0.9		1246	704.1	3.89	586.2	504.7	990
0.92		1217	719.1	3.93	584.6	499.6	1007
0.925		1209	720.1	3.91	586.8	501.4	1013
0.94		1189	735.0	4.06	572.9	486.9	1016
0.95		1178	742.6	3.88	595.6	504.7	1045
0.96		1164	748.9	4.01	581.6	491.3	1041
0.975		1134	753.0	3.83	601.1	505.2	1073
1.0		1113	780.0	3.94	596.8	497.3	1094
1.02		1088	778.0	4.0	590.6	489.4	1103
1.04		1061	800.0	3.99	594.2	488.9	1125
1.06		1037	811.2	3.93	602.4	492.4	1150
1.08	↓	1002	818.3	3.95	599.0	485.8	1167

5.0 DISCUSSION OF RESULTS

5.1 SUMMARY CURVES

Volume 1 presents more than 3500 octave band SPL-versus-frequency curves arranged in an orderly sequence to cover the various transducer locations, model attitudes, and wind-tunnel conditions. This information is summarized here in Figures 8 to 11. Additional data are presented in Volume 1 for two categories not included in the summaries: (1) the supersonic data, which were very low in level, and (2) the data taken with the model oriented at 90 degrees in the Ames test.

The octave band sound pressure levels for various Mach numbers for 16 positions on the model are shown in Figure 8. The positions chosen demonstrate the relative dependence of SPL on Mach number encountered at locations near different vehicle contour features. Typically, the curves increase in level at a rate of 3 db per octave, reach a broad peak, then drop off at higher frequencies. The frequency for the peak octave band level and the maximum level reached are strongly dependent on Mach number and on location relative to vehicle contouring. As the Mach number is increased, there is a tendency for the overall level to increase and for the frequency at which the peak level occurs to be progressively lower. At a "critical" Mach number the level drops off abruptly and the spectrum again peaks at a higher frequency. Large changes in level and peak frequency resulting from Mach number changes are observed downstream of a shoulder, such as at Positions A-27 and B-2. In contrast, for positions where there is little change in contour, the maximum level reached is much lower, and there is less change in level or peak frequency with a change in Mach number (e.g., B-4 and A-20).

Figure 9 shows the variation in overall SPL observed at fixed Mach numbers as a function of angle of attack. For regions of the vehicle where the influence of Mach number on SPL is small (i.e., not near vehicle contour changes), variations in SPL with changes in α for a given Mach number are likewise small. For these locations and at a fixed Mach number, a small upward trend (about 2 db per 10 degrees) in SPL with change in α is indicated as α brings the location to the leeward side (B-4, B-5, B-10, B-12). For a transducer located near a shoulder and for the Mach number range in which the SPL is highly dependent on Mach number, the SPL varies appreciably with angle of attack at a fixed Mach number (B-1 at Mach 0.8 and 0.85). This apparently results from the change in shock location with respect to the transducer for a fixed Mach number. Although no general trends with α are discernible for locations near contour changes, it is believed that varying α has little effect on the maximum levels reached at a particular location; i.e., angle of attack changes only alter the Mach number at which the maximum SPL occurs for a given position on the vehicle.

The ratio of overall rms pressure to dynamic pressure is plotted in Figure 10, with the ratio values expressed in direct and in decibel form. These values are plotted versus Mach number for different positions on the vehicle. The data shown

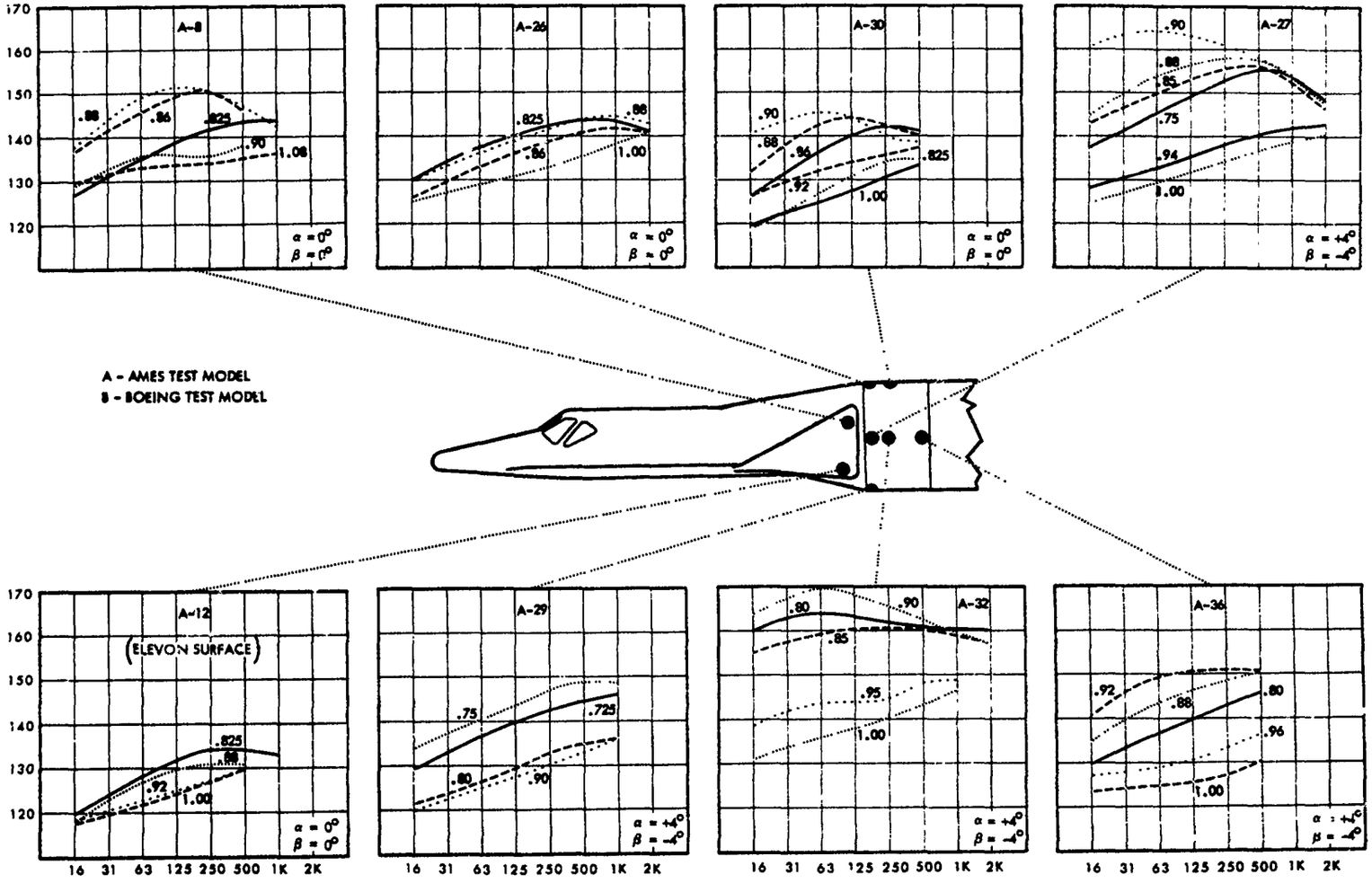

Figure 8: Octave Band Sound Pressure Levels for Various Mach Numbers at Different Positions on the Vehicle.

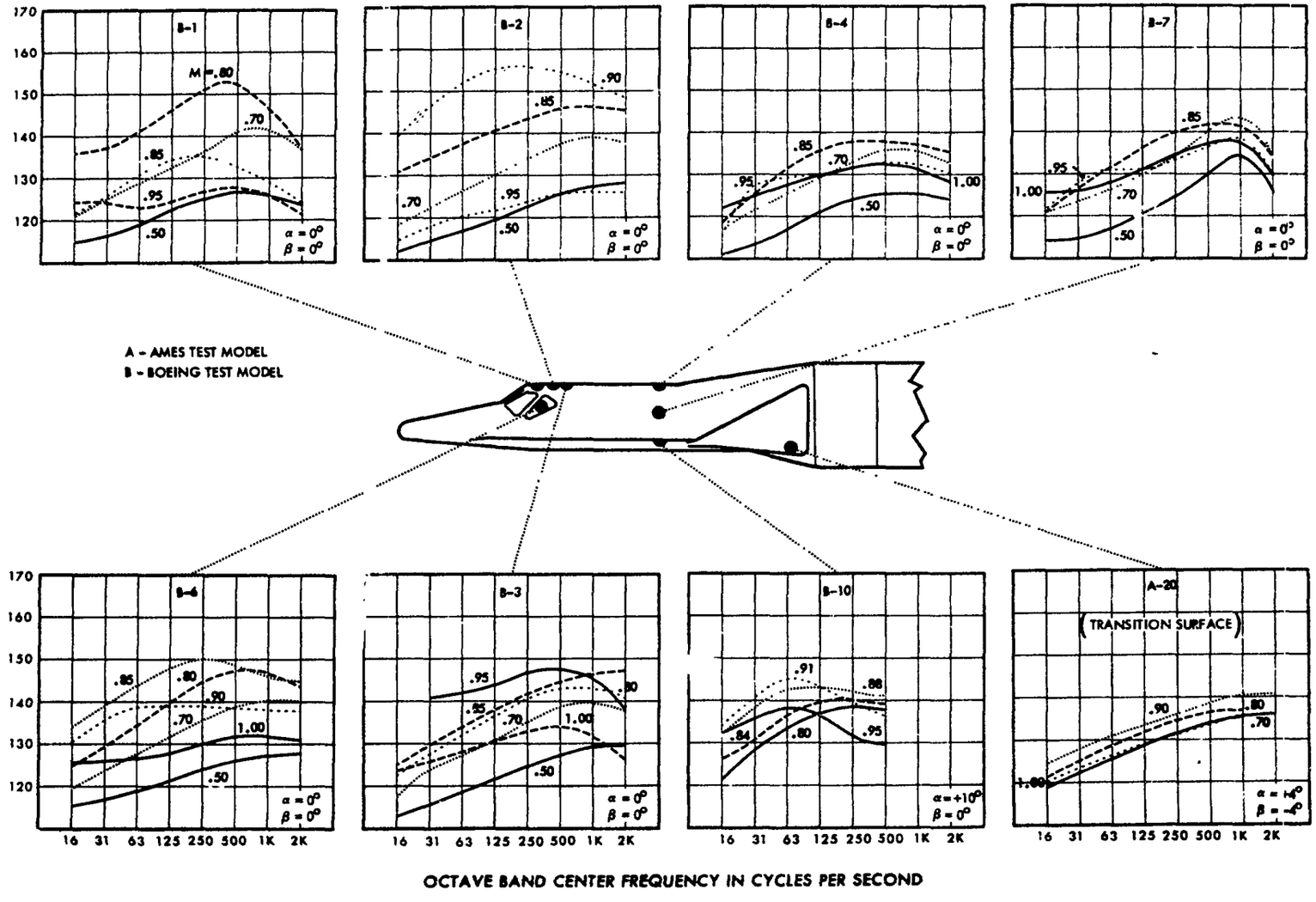

Figure 8 (Cont.)

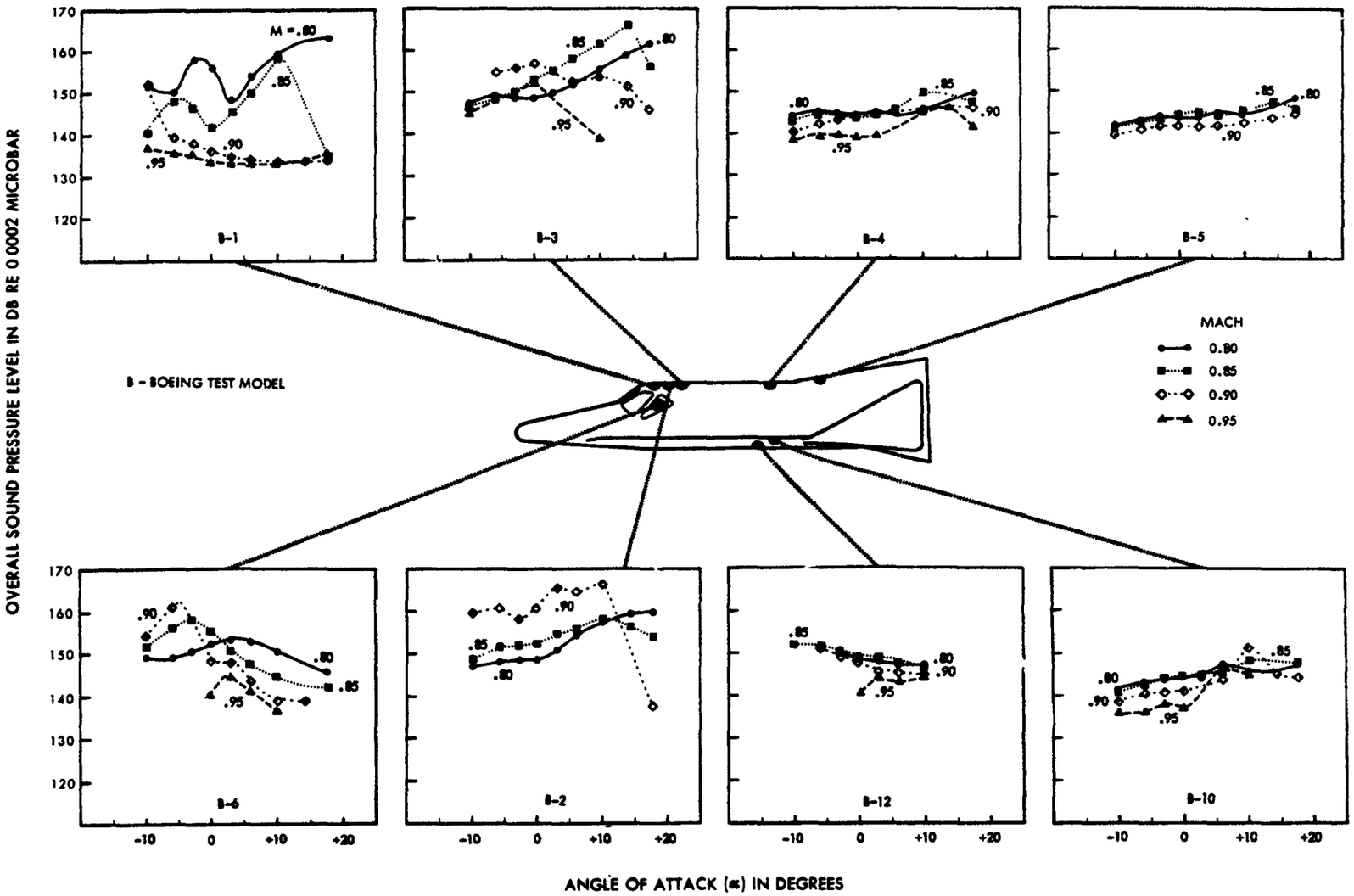

Figure 9 : Variation of Overall Sound Pressure Level with Angle of Attack for Different Mach Numbers.

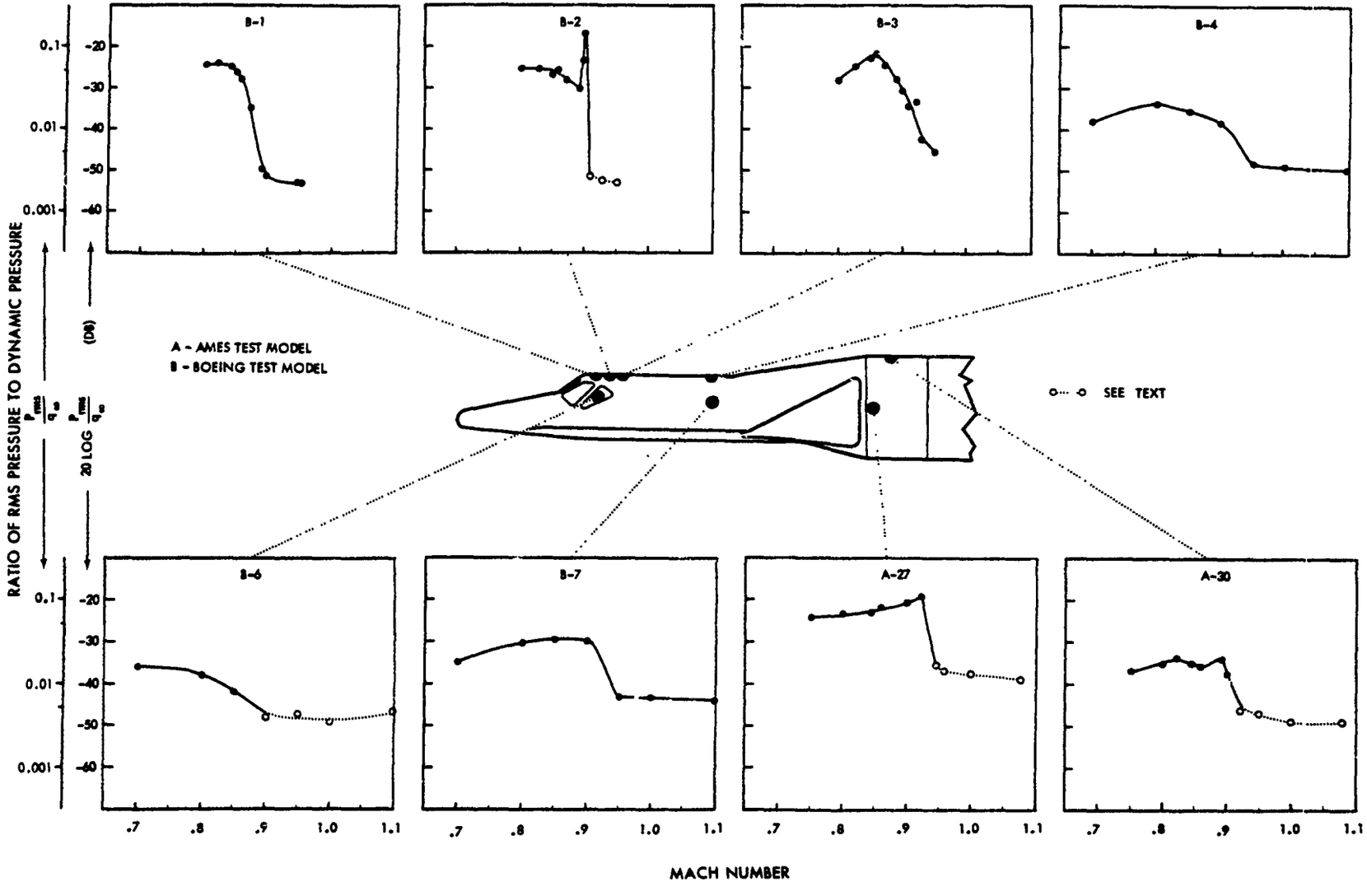

Figure 10: Variation of Normalized RMS Pressure with Mach Number for Eight Vehicle Locations.

are typical for microphone locations where overall rms pressure varies significantly with Mach number. Progressing upward in Mach number, the curves show relatively high p_{rms}/q_∞ values; then, a significant drop occurs often quite abruptly at a "critical" Mach number. The free-stream Mach number associated with this abrupt change in level is typically in the range of 0.85 to 0.90. A typical maximum p_{rms}/q_∞ value for locations downstream of a shoulder is 0.1 (i.e., about 25 db above the nominal value of 0.006 associated with boundary-layer noise for attached flow). For Mach numbers above the critical value, the p_{rms}/q_∞ ratios are on the order of 0.006, although considerable variation from this value is observed for specific locations. Difficulties resulting from low signal-to-noise ratios for portions of the test prevented obtaining accurate high-frequency data at some of the highest Mach numbers when the sound pressures were low. In these cases, estimates of the high-frequency portion of the spectra were made to obtain the overall SPL for determining p_{rms}/q_∞. Where the high-frequency portions of the spectra were estimated, these p_{rms}/q_∞ values are indicated by open symbols in Figure 10.

The total range of octave band sound pressure levels observed at 16 locations on the vehicle during the transonic tests are shown in Figure 11. Data in this figure cover the total range of angles of yaw, elevon and rudder deflection, and ±4-degree angle of attack range, for the Mach number range of 0.7 to 1.08. Extremely large variations in level are seen for locations on the vehicle near contour changes the largest ranges being associated with the lower frequencies. An inspection of Figure 8 will show that a large portion of the total octave-band SPL variation results from Mach number changes. The large range in octave-band sound pressure levels illustrates the difficulty of attempting to predict accurately the levels for a particular flight condition and vehicle location.

5.2 ELEVON AND RUDDER EFFECTS

The Boeing transonic tunnel test covered a wide range of elevon and rudder settings. Data from each microphone location were examined where possible for fixed Mach number and model attitude values (but different elevon and rudder settings), to determine the effect on the SPL at a given location. Except at Location B-11, the effects of elevon and rudder settings were negligible.

5.3 REPEATABILITY OF DATA

Considering microphone locations other than B-11, the repeated Mach numbers and model attitudes may be viewed as repeated test conditions for the purpose of evaluating the merit or confidence of a single data sample. Table 4 shows the variation of the octave band measurement from the mean value when three or more repeated (except that elevon and rudder settings vary) conditions were available for comparison. Octave-band SPL variations for different microphone locations, Mach numbers, and angles of attack are included in the results of Table 4. The octave-band sound pressure level measurements include possible variations that occur in the tunnel conditions, model settings, and data recording and

Table 4 : Repeatability of Data for Boeing Transonic Tunnel Tests

OCTAVE BAND CENTER FREQUENCY (CPS)	PERCENT OF DATA WITHIN INDICATED DECIBEL RANGE OF THE MEAN OF THREE OR MORE MEASUREMENTS		
	± 0.5 DB	± 1 DB	± 2 DB
16	42.5	69.5	91
31.5	51.5	79.5	95.5
63	55	80.5	94.5
125	64	85	96
250	64	84	96
500	49	79	96
1000	55	82.5	96.5
2000	69.5	86.5	96

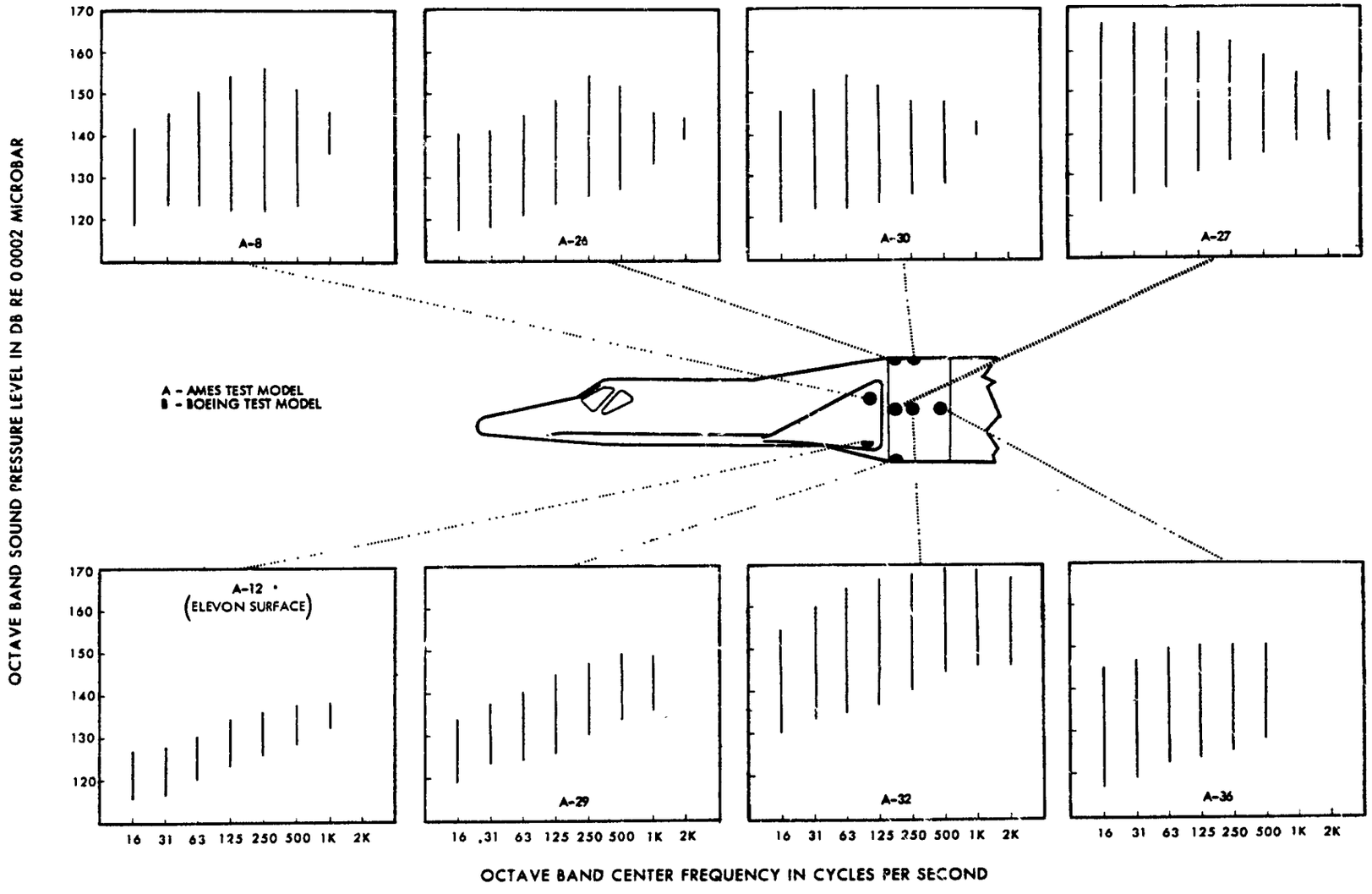

Figure 11 : Range of Octave Band Sound Pressure Levels Covering the Total Ranges of Yaw Angle and Elevon and Rudder Deflection, and a ± 4° Angle of Attack Range for the Mach Number Range of 0.70 to 1.08.

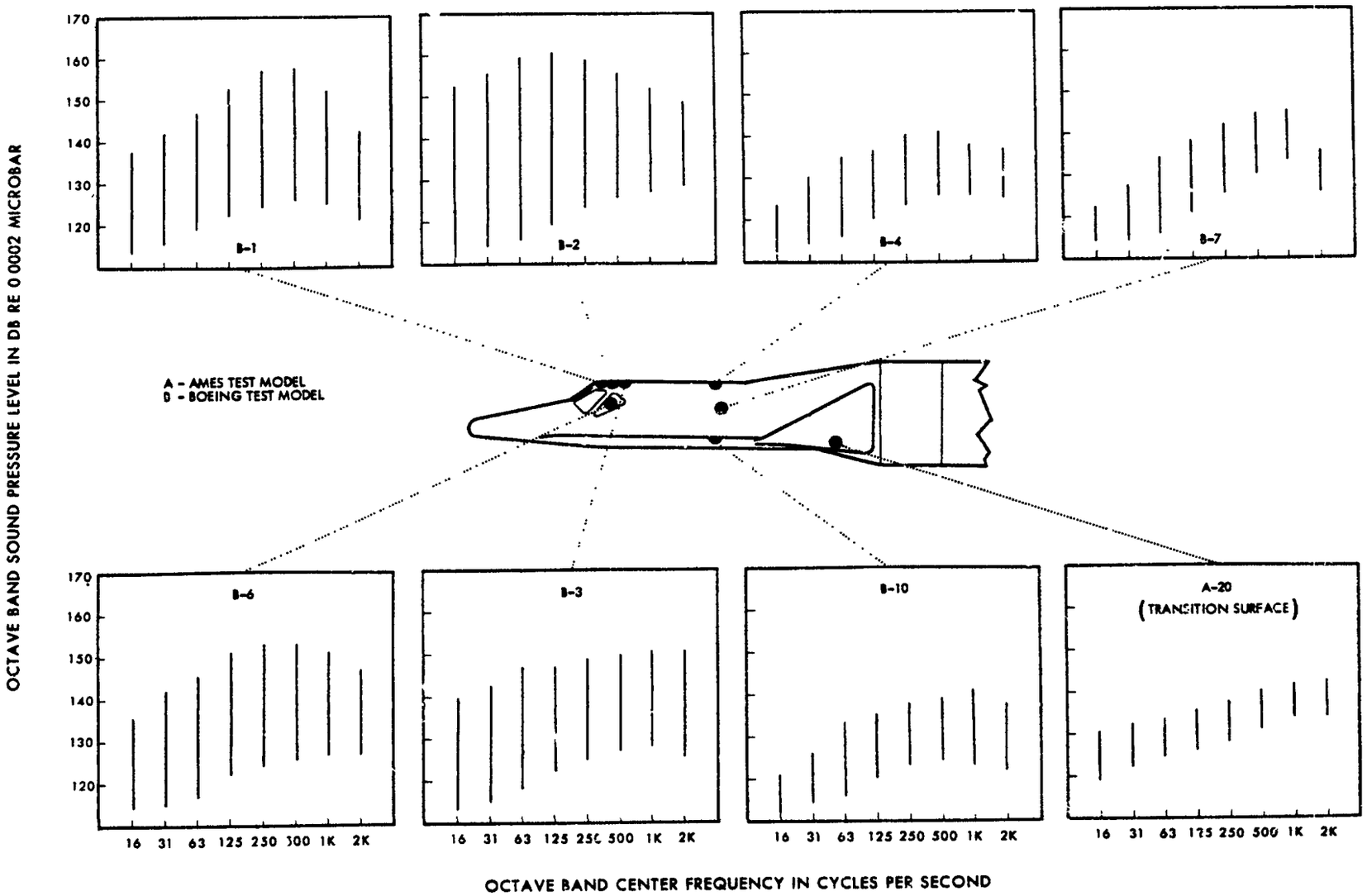

Figure 11: (cont.)

reduction. The data in Table 4 were based on approximately 350 readings per octave band. From the table, it can be seen that for repeated data runs, about 95 percent of the octave-band SPL measurements fell within ±2 db of the mean of three or more measurements.

5.4 LOCALIZED PRESSURE CHARACTERISTICS

The pressures on the model resulting from the unsteady flow alternations brought about by the shock wave interacting with the boundary layer tend to be highly localized and significantly change their character either at a fixed location for small changes in Mach number, or at a fixed Mach number for small changes in location. Data presented in Figures 12, 13, 14, and 16 from Microphones B-1, B-2, and B-3, located aft of a shoulder on the pilot's canopy, illustrate the local nature and complexity of this type of fluctuating pressure source.

Figure 12 shows the variation of space correlation coefficients, measured in octave bandwidths, for Microphones 1 with 2 and 1 with 3 as a function of Mach number (Figure 12 (a-c)) and as a function of microphone separation distance (Figure 12 (d-f)) for three different octave bands. The important features of these curves are as follows:

1) For the two lower octave bands shown, the correlation between Microphones 1 and 3 becomes increasingly and significantly negative as the Mach number is increased, up to about Mach 0.86; then, at higher Mach numbers, the correlation becomes approximately zero or somewhat positive.

2) Microphones 1 and 2 tend to be uncorrelated for the lower Mach number range; then, they show a positive correlation (about 0.7) for Mach numbers above 0.9.

3) For the Mach number where the SPL is highest ($M \approx 0.84$ for Microphone 1), high positive correlation (> 0.5) exists for only a small distance downstream (< 0.5 inch for this particular model).

The variation with frequency of the negative correlation seen in Figure 12 for Microphone B-1 with B-3 is shown in Figure 13 for Mach 0.86, with associated SPL spectra. The correlation coefficient data shown were measured with 1/9th, 1/3rd, and full octave bandwidths. The agreement among the three measurement bandwidths is good, indicating that very little important detail is lost in using octave band analysis for this type of noise.

The pressure events producing the negative correlation shown in Figure 12 between Microphones 1 and 3 can be seen in Figure 14, which shows simultaneous pressure histories from Microphones 1, 2, and 3 at Mach 0.87. Significant correlation between Microphones 1 and 2 or 2 and 3 is not apparent. The pressure history from Microphone 2 appears as an ordinary random-amplitude noise signal expected for turbulent-flow noise. The traces for Microphones 1 and 3 also show a random-amplitude noise character but in addition have pressure pulses characteristically resulting from alternating attached and separated flow states.

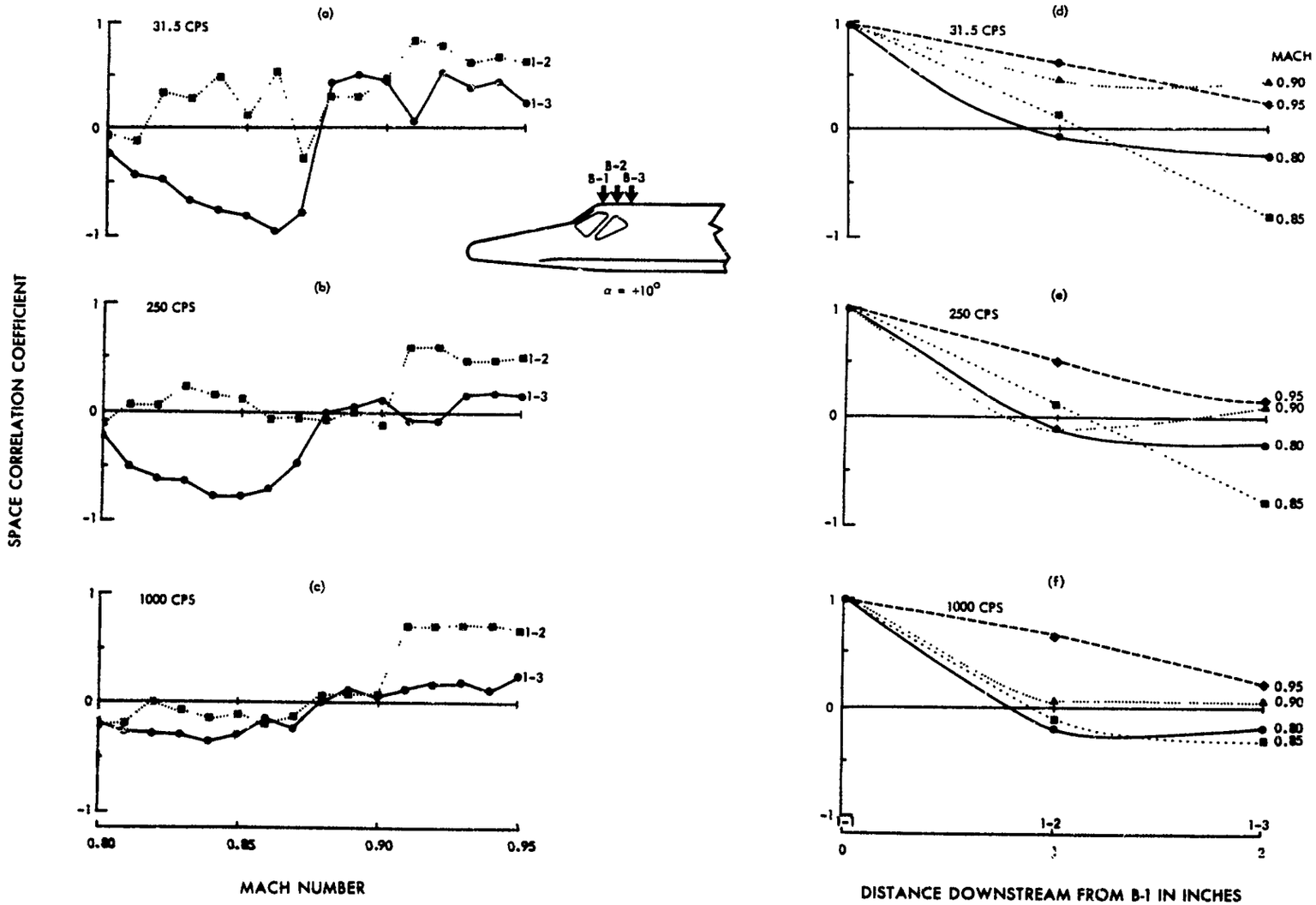

Figure 12: Space Correlation Coefficient Measurements (Octave Bandwidths) for Three Positions on X-20 Canopy, With B-1 as Reference Transducer

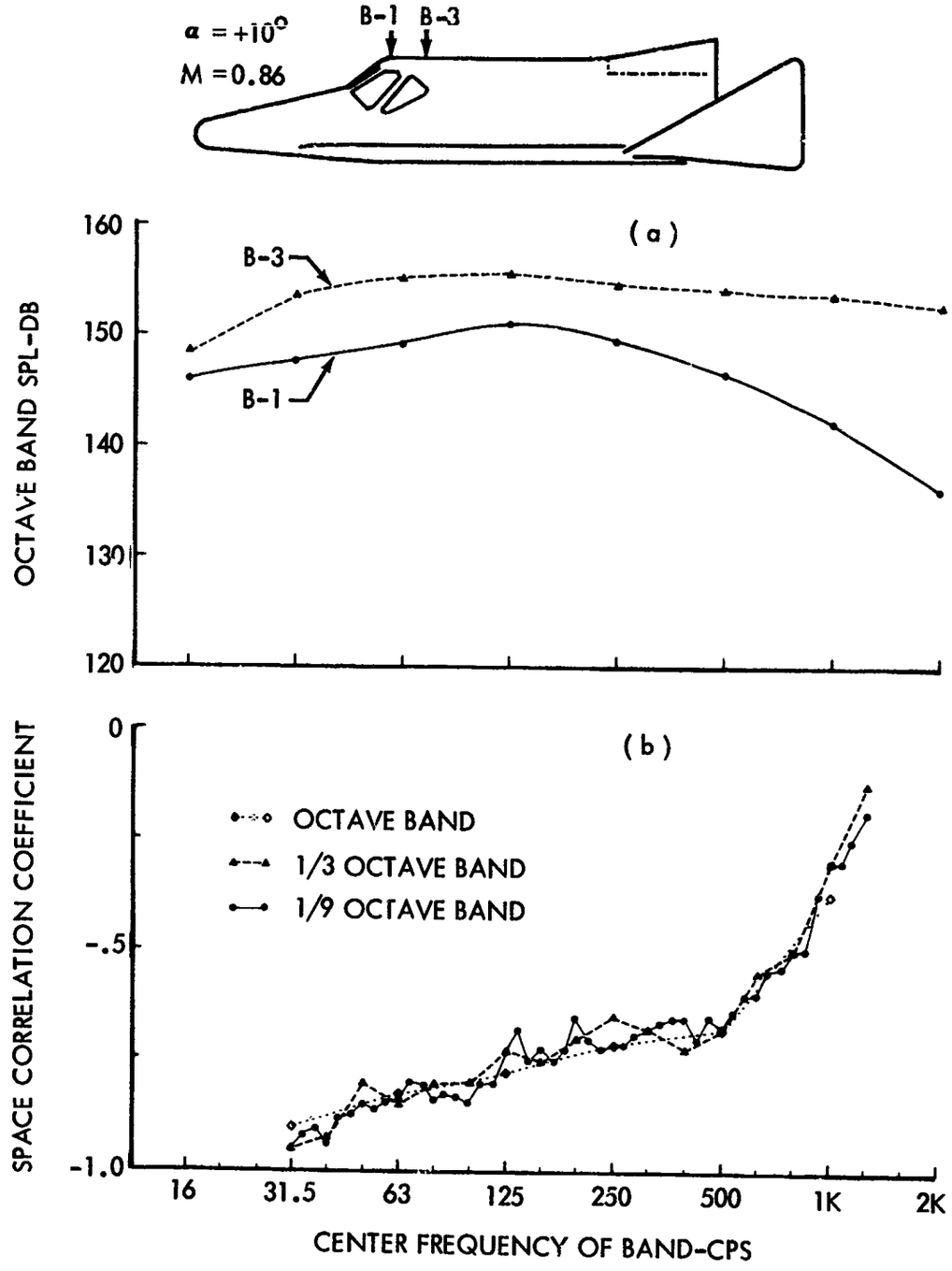

Figure 13: Comparison of Data from Two Microphone Locations Downstream of a Shoulder (a) Octave Band Sound Pressure Level Versus Frequency (b) Space Correlation Versus Frequency for Three Analysis Bandwidths.

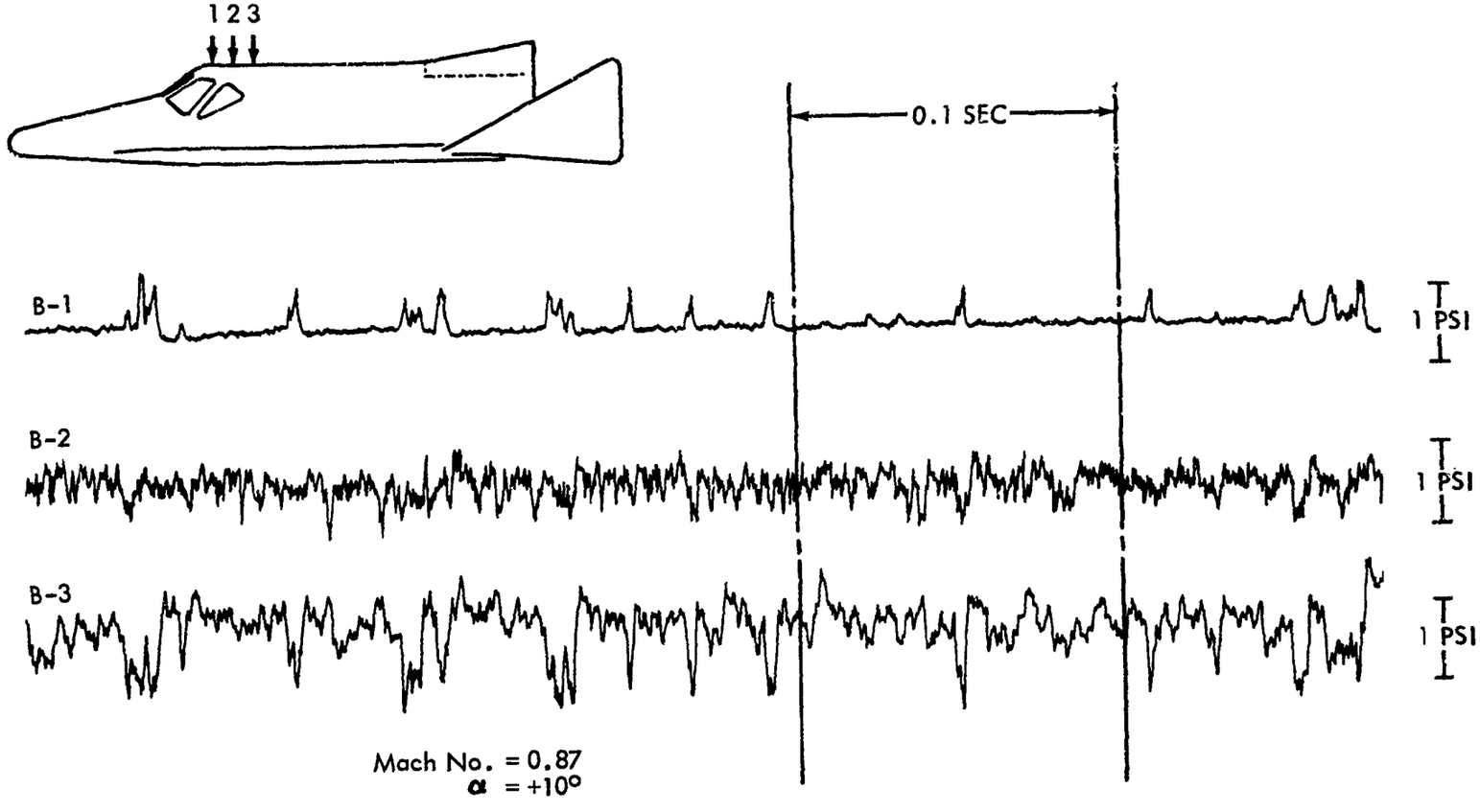

Figure 14: Simultaneous Pressure Histories for Microphone Positions B-1, B-2, B-3.

These pressure pulses are in opposite directions for the two traces, giving rise to the negative correlation measured between Microphones 1 and 3 for the lower Mach numbers.

Similar pressure pulses are present in the pressure histories observed aft of the X-20 transition section at Mach numbers characteristic of the highest SPL conditions. Short samples of different types of pressure histories with their associated octave-band SPL-versus-frequency data are shown in Figure 15. Observed high-level, low-frequency spectra do not always exhibit a rectangular wave character as shown for A-27; some tend to have low-frequency pressure fluctuations and exhibit wave forms similar to that shown for A-32. These low-frequency pressure fluctuations presumably are due to changing flow conditions or are a result of a complicated interaction of the shock wave with the boundary layer at or near separation. The upper two pressure histories shown in Figure 15 for microphones aft of the X-20 transition section probably result from alternating flow situations or shock oscillation; the lower pressure trace, for a microphone located on the rudder, shows random noise typical of that produced by the passage of turbulent eddies in the boundary layer. Considerable energy is present at the low frequencies for the upper two traces, the spectra peaking at approximately 20 cps and 63 cps, respectively. The lower level spectrum (A-8) corresponding to the random pressure history is peaking at 500 cps or higher.

The frequency for the spectrum peak and the octave band SPL associated with this peak frequency are plotted versus Mach number in Figure 16 for locations B-1, B-2, and B-3. At Mach 0.8 these microphones sense high levels; this is followed by a large drop in level at Mach numbers of 0.88, 0.91, and 0.93, respectively. Just prior to this rapid change in level with Mach number, there is a large increase in the low-frequency content of the pressure spectrum as shown by the shift of the spectrum peak to lower frequency. At higher Mach numbers ($M \approx 0.95$) the frequency for the spectrum peak shifts back to a high value, and the level remains low. The peak frequency for Microphone B-3 shifts with increasing Mach number to lower frequency, back to higher frequency again, lower frequency again, and then returns to a high frequency. A possible explanation for this particular action is presented as part of the discussion that follows.

The high level of the rms pressure fluctuations for these three locations, together with pressure histories (Figure 14) showing pressure jumps, suggest the presence of unsteady shock-wave/boundary-layer interaction. The negative correlation of the pressure jump in signals from B-1 and B-3 and their lack of correlation with signals from B-2 at low Mach numbers, followed by the tendency toward positive correlation of all three microphones at higher Mach numbers, indicate a localized complex-flow condition is present about the three microphones. A flow model such as a shock-induced separation bubble can be employed to rationalize the data of Figures 12, 13, 14, and 16. For Mach numbers near 0.86, the local flow conditions about the microphones are sketched in Figure 17 (a,b).

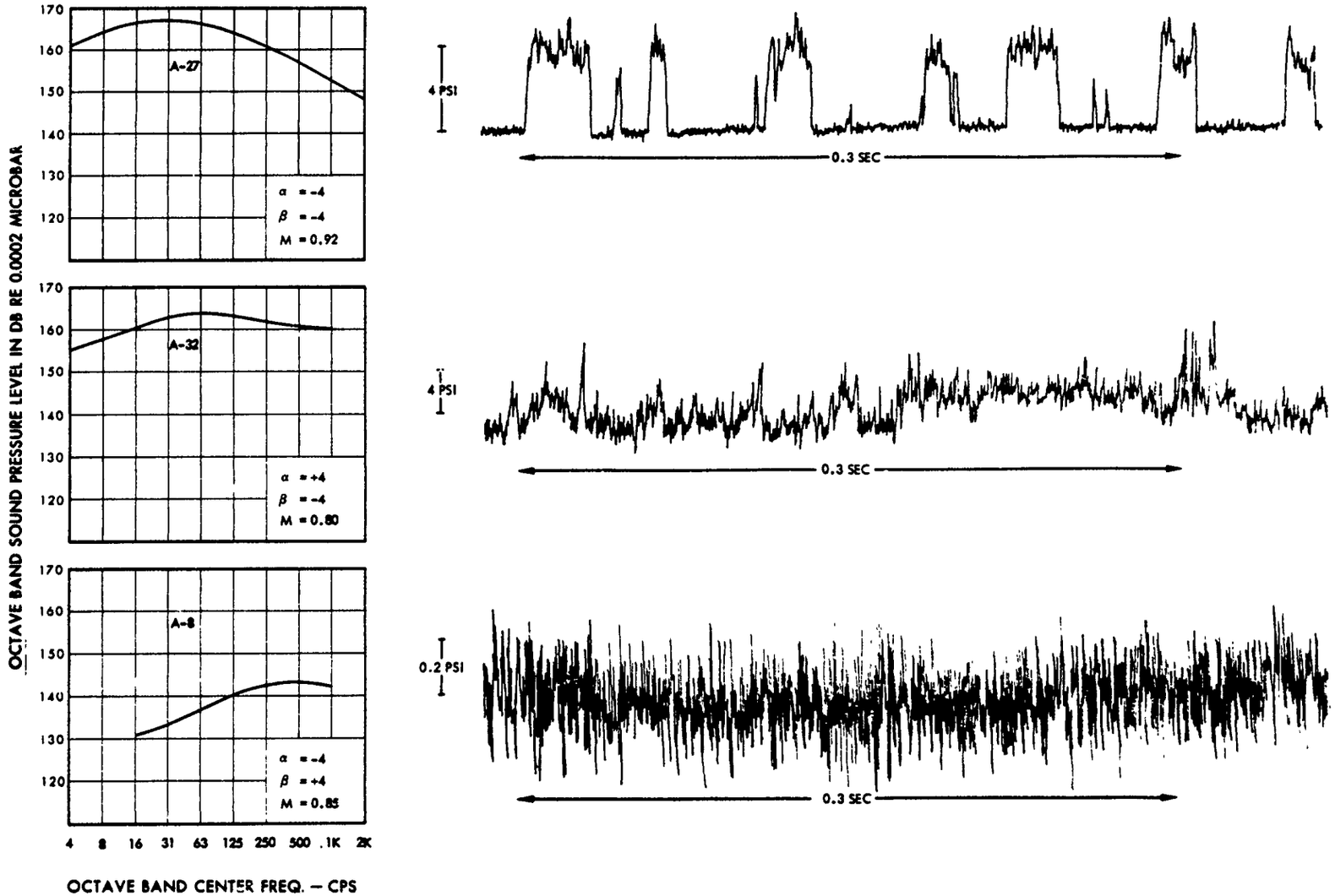

Figure 15: Comparison of Pressure Histories With Associated Octave Band Sound Pressure Levels for Three Different Types of Pressure Variations.

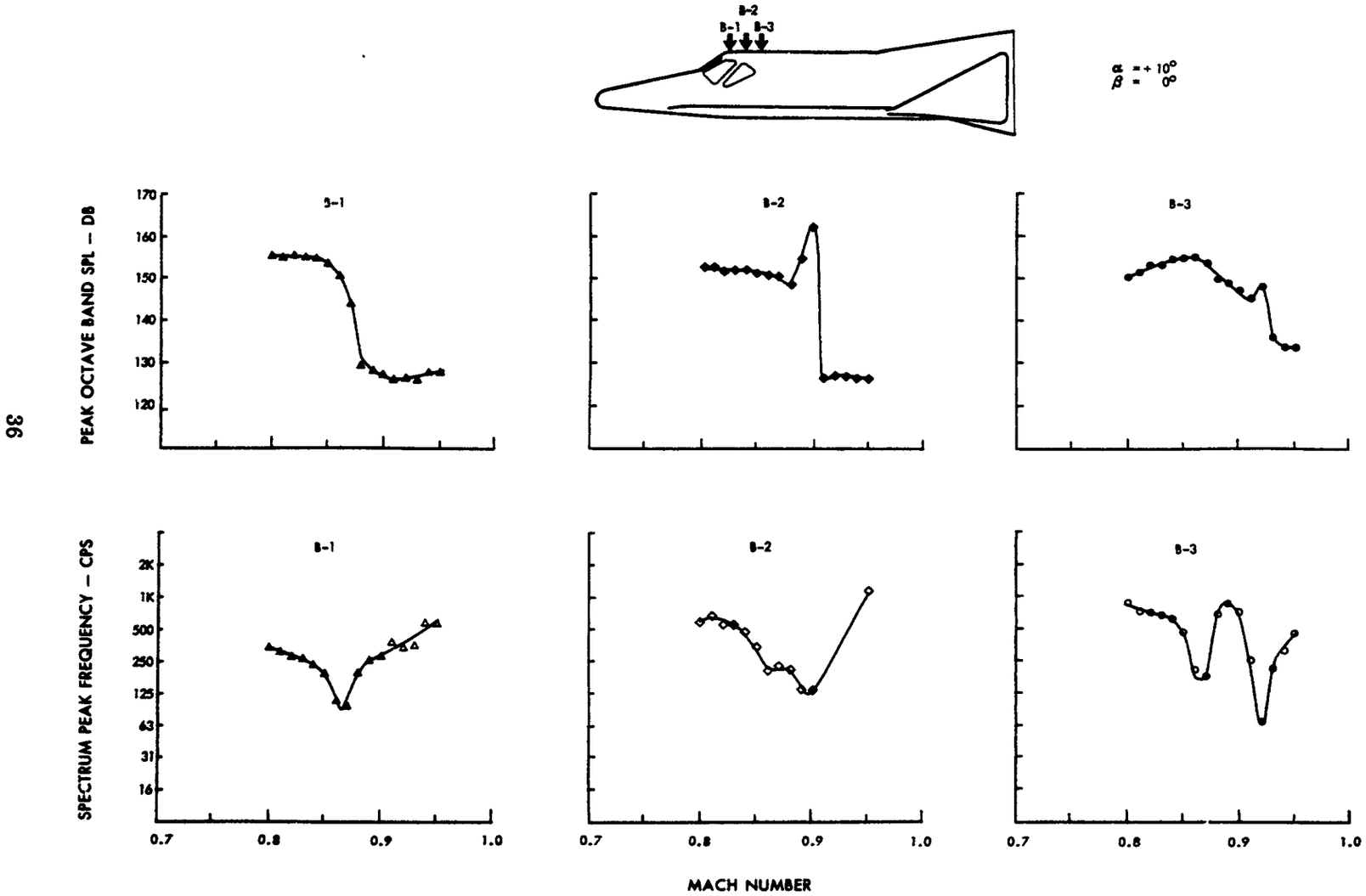

Figure 16: Variation of Sound Pressure Level and Spectrum-Peak Frequency With Mach Number

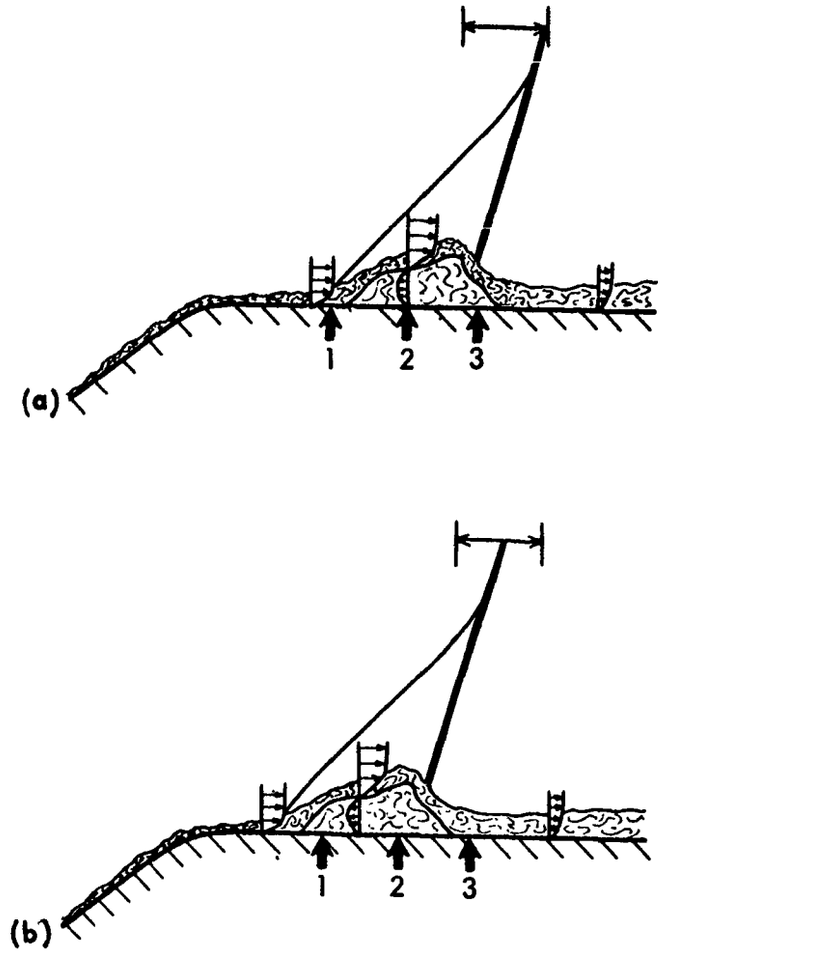

Figure 17: Sketch of Local Separation and Resulting Pressures

Flow conditions alternating between (a) and (b), caused by fore and aft oscillation of the shock-wave attachment point, produce signals (at the three microphones) that appear as sketched in (c). The observed negative correlation between Microphones B-1 and B-3 results from the pressure-jumping portion of the fluctuating pressure. With increasing Mach number, this pressure system moves downstream, and the pressure jump ceases to occur first at Microphone B-1; therefore, above Mach 0.87, B-1 senses a drop in SPL and a shift to a high-frequency spectrum that is characteristic of attached turbulent flow.

Microphone B-2 then senses the fluctuating mean pressure at about Mach 0.90, with the resulting high-level spectrum peaking at low frequencies. As the Mach number is further increased, B-2 is within the attached portion of the flow upstream of the shock; it now senses high-frequency, low-level pressures. Microphone B-3, which initially (at Mach 0.86) was receiving pressure fluctuations caused by the downstream portion of the separation bubble, next (as Mach number increases to about 0.89) senses pressures characteristic of the center part of the bubble. Then, at Mach 0.92, a fluctuating mean pressure is sensed a second time as the upstream attachment point moves by. Since the fluctuating mean pressure condition occurs twice (Mach 0.86 and 0.92) at B-3 it twice causes a drop in peak frequency of the spectrum, separated at intermediate Mach numbers by peak frequencies characteristic of the separated flow region upstream of the foot of the shock. At higher Mach numbers, the shock wave moves downstream and the three microphones are in the attached-boundary-layer flow region (i.e., low-level pressure fluctuations with spectrum peaks at relatively high frequencies). At these Mach numbers, some positive correlation exists due to the microphones' proximity in the moving pressure field presented by the convected eddies of the boundary layer.

Although the flow model of locally separated flow occurring near a fluctuating shock appears consistent with the fluctuating pressure data recorded for Microphones B-1, B-2, and B-3, without detailed flow measurements it must be considered as a hypothesis at present. Means for determining flow patterns were not included in the X-20 wind-tunnel tests because these were beyond the scope of the program, which was to determine sound pressure levels at specific locations on the vehicle. To define adequately the flow conditions that exist, boundary-layer velocity profiles, Schlieren photographs, and static-pressure distributions are required.

5.5 POWER SPECTRAL DENSITY ANALYSIS

In addition to the octave band measurements, power spectral density measurements were made from magnetic tape recordings representative of the different types of pressure histories recorded, to verify experimentally the absence of discrete frequencies in the data. Typical measured results are shown in Figure 18, with power spectral density curves obtained by mathematically converting octave-band measurements to the PSD form.

Data for Position A-27, which is downstream of a shoulder with a 26-degree shoulder angle, is selected for further analysis. An oscillographic pressure

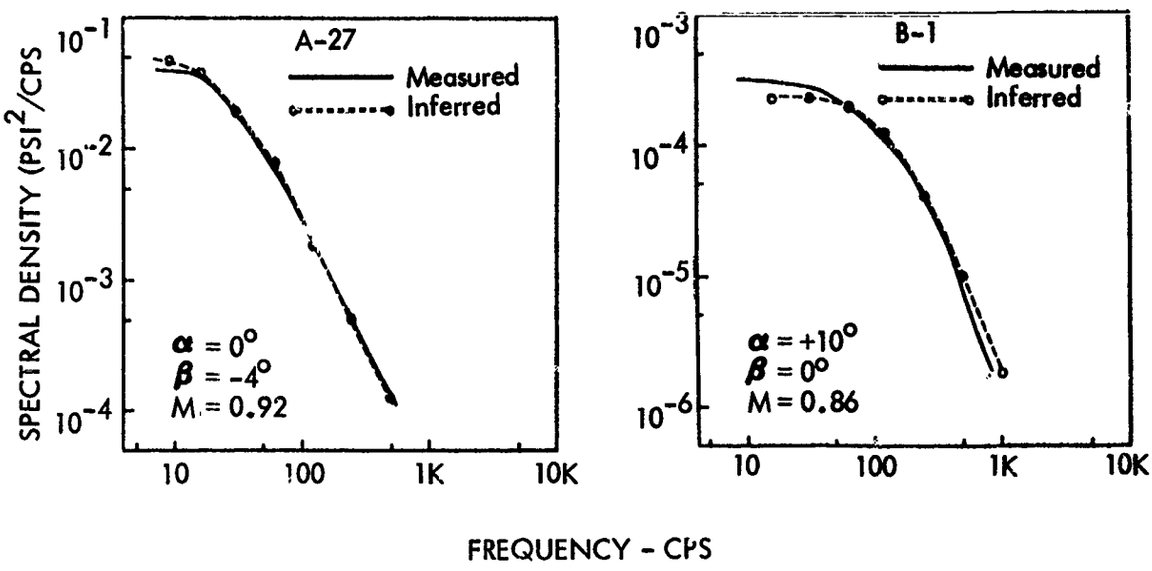

Figure 18: Power Spectral Density Measurements of Buffet Pressures for Two Different Microphone Positions Compared with PSD Values Inferred from Octave-Band Measurements

history for a short sample of noise taken at Mach 0.92 (a maximum level condition) is shown in Figure 19(a). The significant feature of this trace, as distinguished from a trace of normal random noise, is that the signal appears to switch rapidly between two mean pressures at a random rate. As discussed previously, this suggests an unstable flow condition of alternate separation and attachment of the boundary layer. The lower-level random-amplitude signal, which is superimposed on the two mean pressures, is attributed to the random noise associated with the particular flow conditions (i.e., attached or separated).

By considering the idealized case for a signal that alternates between two steady pressure values at random rates, as in Figure 19(b), it is possible to calculate the power spectral density associated with such a signal. A calculation was made by using an expression similar to that for the power spectral density of a random telegraph signal (Ref. 9), except that provision for a preferred pressure value is included. The mean difference between the two mean pressure values and the mean time spent at each value were taken from a long-duration oscillograph record. The calculated curve is shown in Figure 19(c) with a measured power spectral density for the actual pressure history. The reasonably good agreement in overall level and spectral content of the calculated and measured values indicates that a process of random switching between two steady pressures can largely account for the measured results, and that the superimposed lower-level random-amplitude signal does not contribute appreciably to the level determination. This supports the theory that the alternating separation and attachment of the flow is the cause of the very intense fluctuating pressures at low frequencies that are observed downstream of convex corners.

5.6 AMPLITUDE DENSITY ANALYSIS

Amplitude density measurements were made for pressure signals typical of the different spectra recorded at different locations and tunnel conditions for the Ames transonic test, from which 45-second recordings were available. Good agreement was obtained between 6-percent-bandwidth measurements and octave band measurements for a few data samples. For convenience, all subsequent measurements were made in octave bandwidths. Typical results for two spectrum types are presented in Figure 20 as the cumulative probability of an instantaneous peak in the signal exceeding a specified peak-to-rms ratio. The straight line included for comparison is the theoretical Rayleigh distribution of amplitudes for narrow-band-filtered Gaussian noise (Ref. 10).

Inspection of Figure 14 shows that Location A-8 has a pressure history and an octave band spectrum typical of random noise for an attached boundary layer. This type noise has an amplitude density that follows closely the Rayleigh distribution (Figure 20). Location A-27 has a high-level, predominantly low-frequency spectrum and a pressure history (Figure 15) typical of the alternating attached and separated flow discussed previously. This type of noise has significantly greater density of high peak-to-rms values for all frequency bands than Gaussian noise (Ref. 7) (Figure 20).

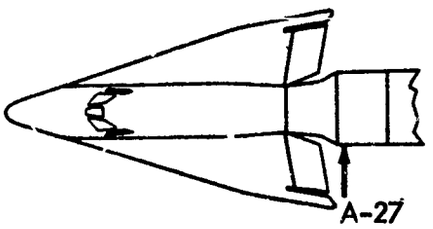

α =-4°
β =-4°
M =0.92

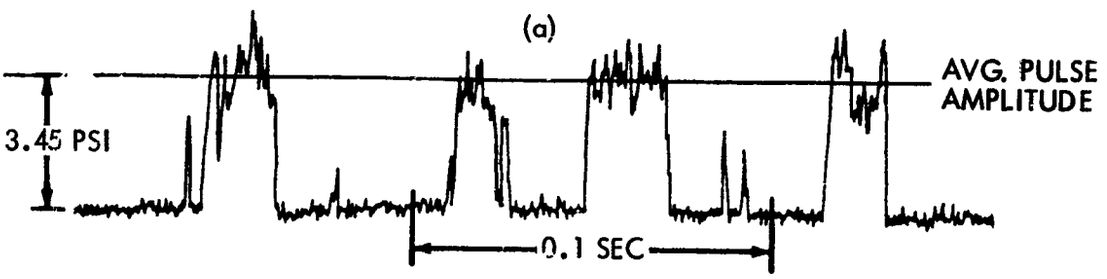

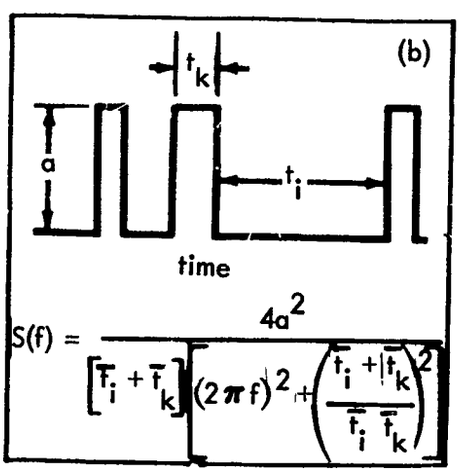

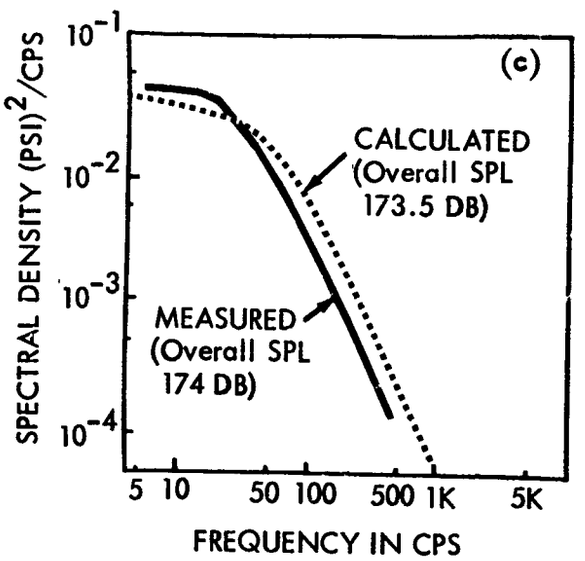

Figure 19: (a) Short Sample of Pressure History, (b) Idealized Wave Shape Used for Calculation, (c) Power Spectral Density Analysis - Comparison of Measured and Calculated

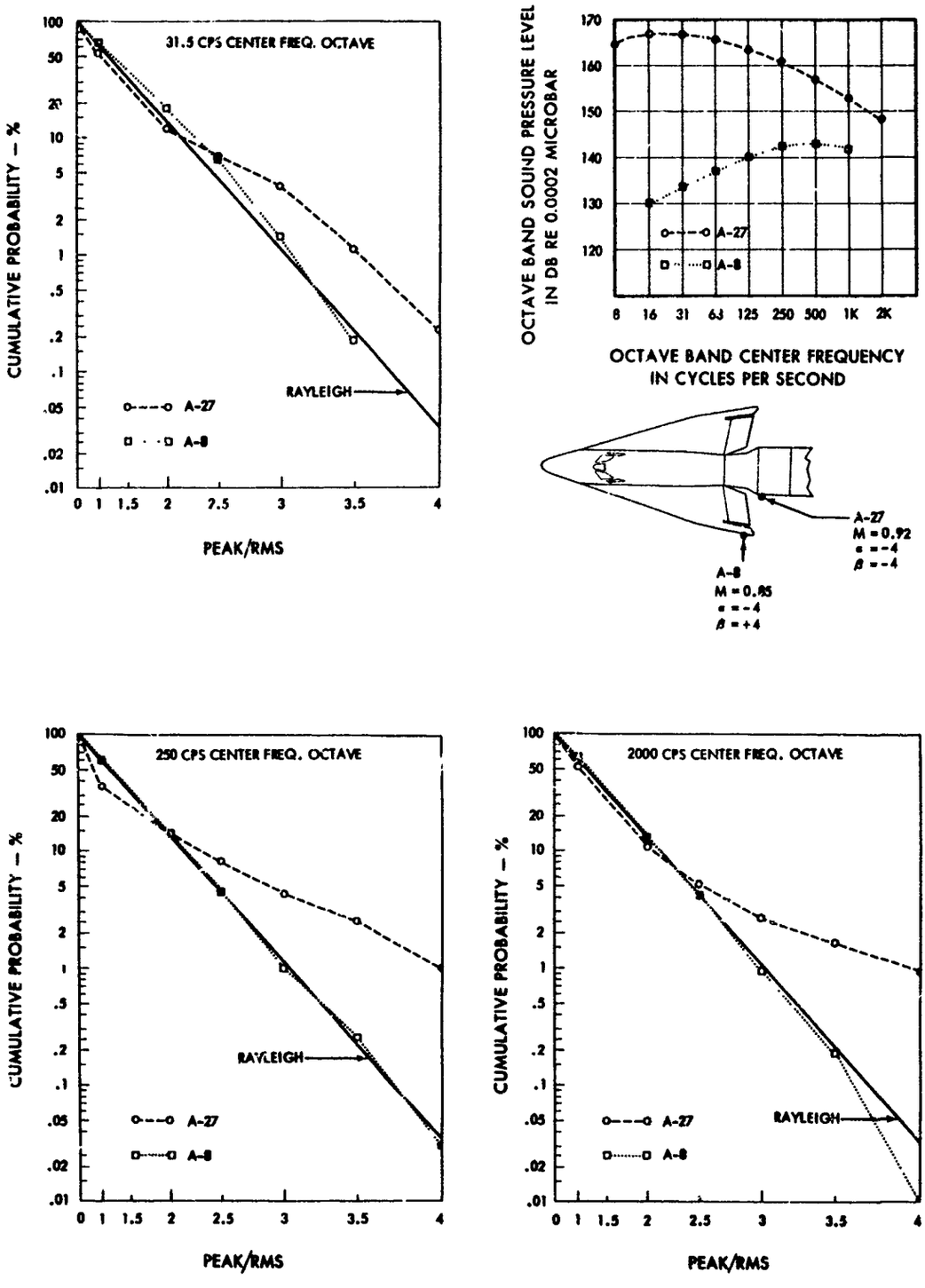

Figure 20: Amplitude Density for Two Different Types of Spectra

5.7 FLUCTUATING BASE-PRESSURE MEASUREMENTS

Data taken for Location B-17 on the Boeing transonic tunnel model for a 10-degree angle of attack indicate that rms fluctuating pressures on a blunt-ended body such as the X-20 can be as high as 5 percent of q_∞. Typical variation of level with angle of attack is shown in Figure 21. Microphones B-15A and B-16A are recessed in the base of the model; levels of about 2 percent of q_∞ were recorded. Although not shown by the curves, the level for these locations does not vary significantly with Mach number.

5.8 GENERAL TRENDS

It is desired to develop general trends for predicting sound pressure levels for application to vehicle design. An examination of the summary curves (Figures 8 to 11) reveals large changes in overall level and frequency for the spectrum peak. These changes often are associated with small variations in Mach number, location on the vehicle, and vehicle attitude. This makes it impractical, at least with present information, to consider predicting the rms pressure level and spectrum for specific flight conditions and specific locations on the vehicle. However, an analysis of the X-20 data, some of the data reported in the literature, and unpublished Boeing data indicates that prediction of maximum overall pressure levels associated with the general transonic Mach number range appears to be possible for some design features. The results of this study are presented in Figures 22 to 28. These figures include the development curves and the resulting design charts, which should be useful in predicting rms pressure levels for designs incorporating transition sections to accommodate larger vehicle cross sections.

The maximum rms pressure levels (in terms of p_{rms}/q_∞) plotted as a function of nondimensional distance (x/d) downstream of a shoulder are presented in Figure 22 for various transition angles (θ). Data for these curves were derived from three wind-tunnel models (Refs. 11 and 12) by selecting the maximum rms pressure levels that occurred at particular x/d values over a range of transonic Mach numbers for each given transition angle. The data for the minimum (8 degrees) and maximum (26 degrees) transition angles of the unsymmetrical X-20-to-booster transition section are included to increase the range of transition angle (θ). The curves shown are for nominally 0-degree angle of attack, although data from the X-20 necessarily included $\alpha = \pm 4$ degrees and $\beta = -4$ degrees. It is believed that small changes in model attitude do not affect the maximum SPL, but only the Mach number at which it occurs. The data presented show orderly trends in the direction expected (i.e., maximum SPL is reduced (1) as distance downstream of shoulder is increased, and (2) as shoulder angle is decreased).

Although in Figure 22 the range of x/d is restricted for the extreme values of θ (8 and 26 degrees), the firmly established trends of the 15- and 20-degree transition angles provide a reasonable basis for extrapolation. Using the data from Figure 22, a set of design chart curves was developed (Figure 23). The significant effect of increasing the transition angle is clearly seen in Figure 23(b) in

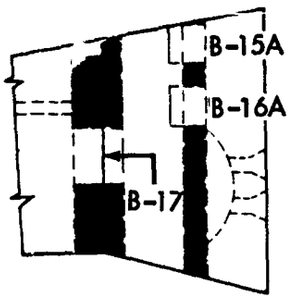

SIDE VIEW - TRANSITION SECTION
(B-17 used only with transition section removed)

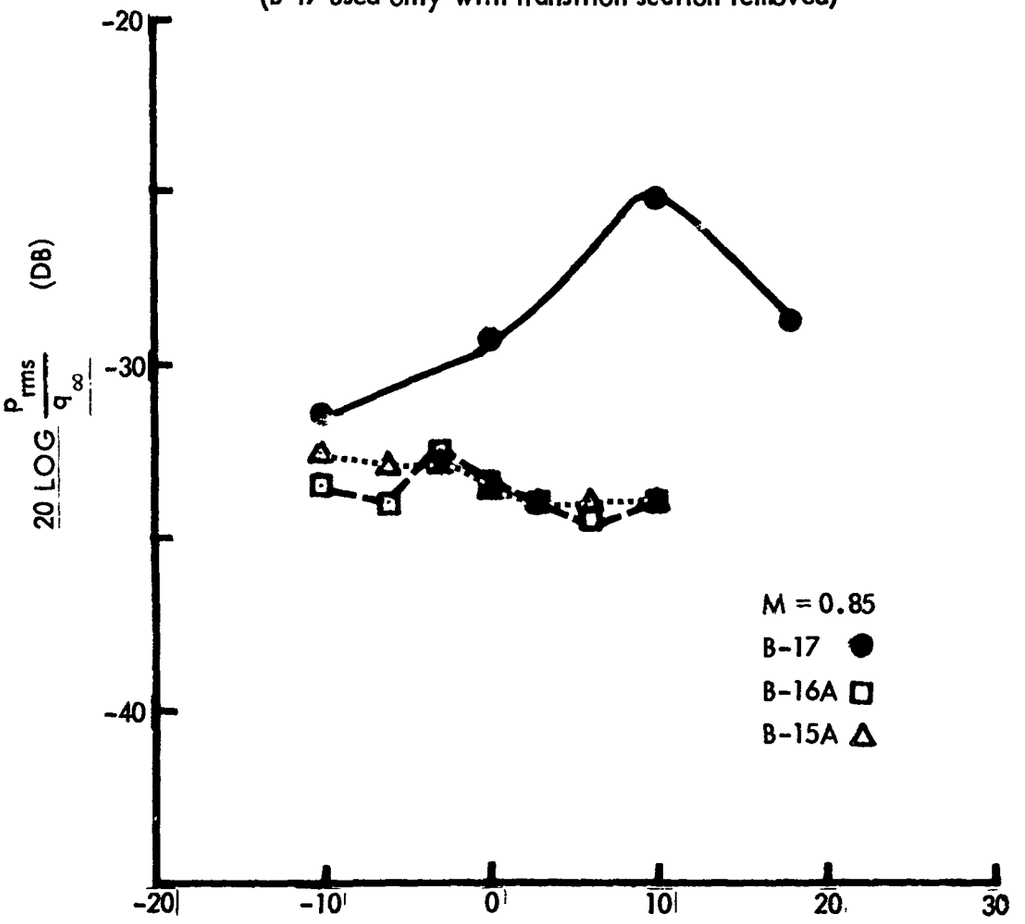

Figure 2 : Normalized RMS Base Pressures Measured on X-20 Model

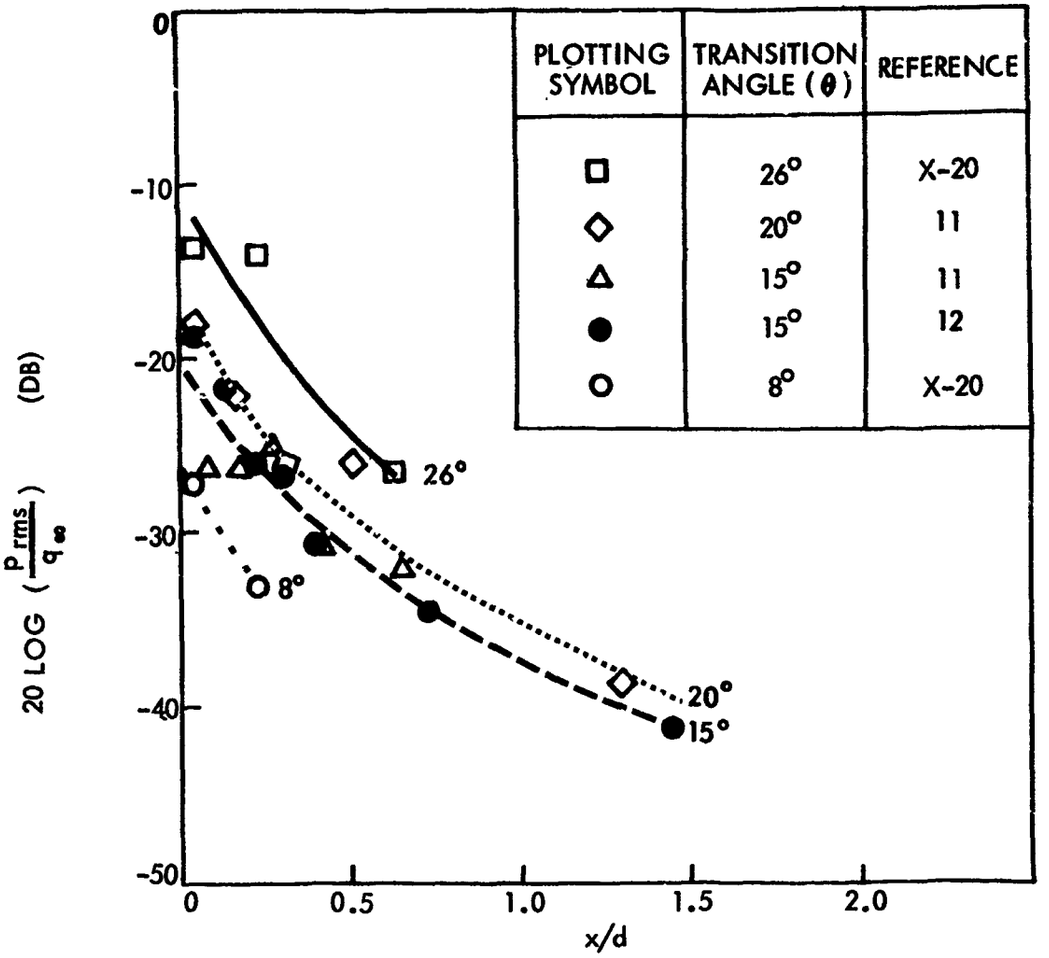

Figure 22: Trends in Maximum RMS Pressure Versus Nondimensional Distance Downstream of Shoulder (x/d) for Four Wind Tunnel Models

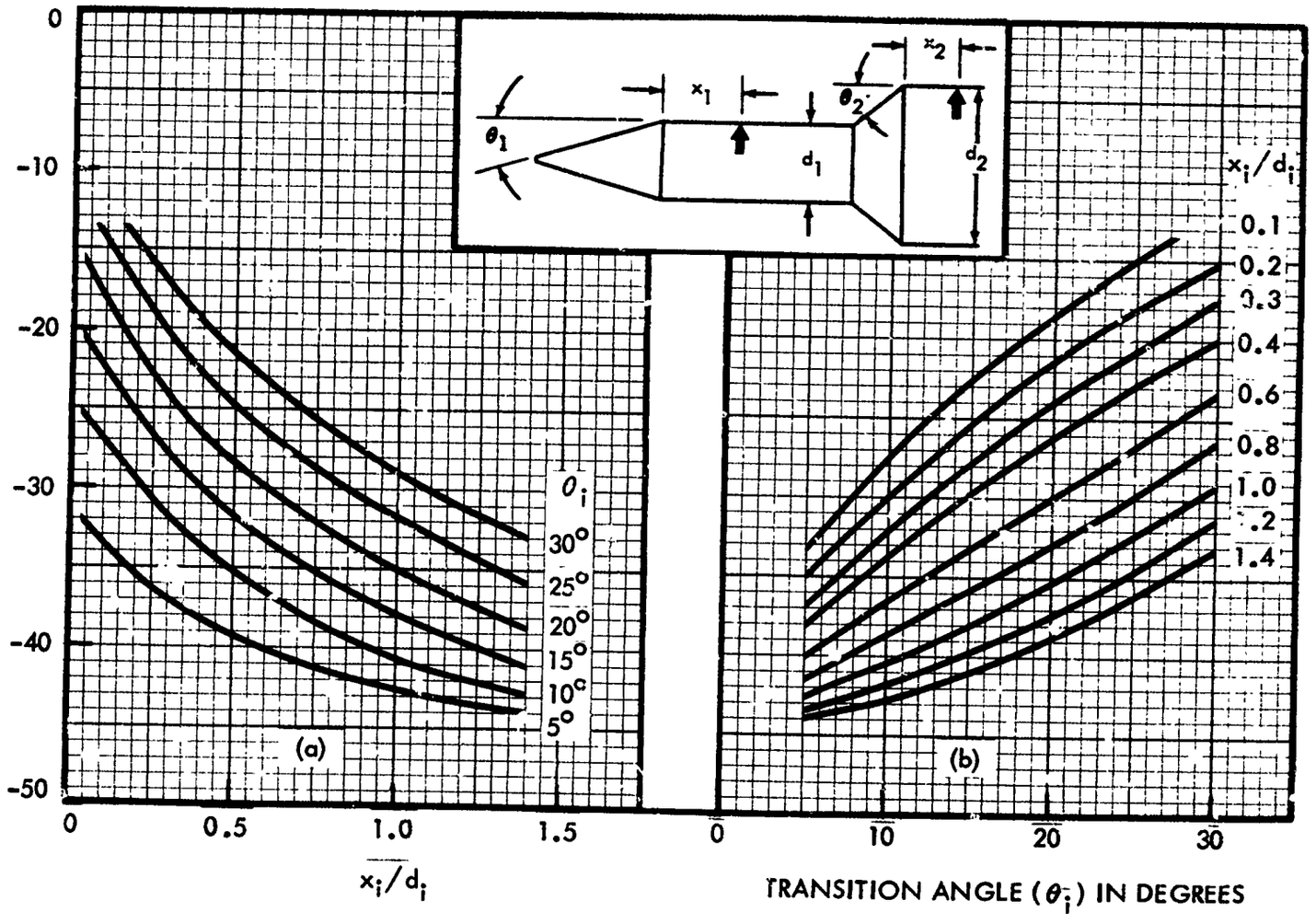

Figure 23: Design Chart for Estimating Maximum Overall RMS Pressure (Encountered in Transonic Conditions) for a Given Transition Angle (θ), Nondimensional Distance Downstream of Shoulder (x/d), and Dynamic Pressure (q_∞)

which it is shown that a 10-degree increase in θ results in an increase in maximum rms fluctuating pressure of approximately 6 db.

Twelve X-20 microphone locations are available to compare maximum SPL values with the design chart of Figure 23. These 12 locations are associated with: (1) the various transition angles formed by the unsymmetrical transition section of the X-20 and the booster (angles noted in Figure 7), (2) the two angles at the pilot's canopy (with and without heat shields), and (3) the several microphone distances downstream of these shoulders. Comparison of the measured maximum sound pressure levels on the X-20 with curves derived from the design chart of Figure 23(a) are shown in Figure 24. A summary of the data agreement is as follows: (1) three-fourths of the X-20 measurements are within ±3 db of the design chart values, (2) the maximum deviation is 6 db, and (3) the mean deviation is -1.3 db.

Several wind-tunnel models that include a variety of diameter and transition angles are presented in the literature (Refs. 11, 13, 14, and 15) for which the location of the maximum SPL can be determined for specific Mach numbers; however, the data given do not include shock location. Reference 16 gives shock location associated with specific Mach numbers for a 1-inch-diameter cone-cylinder model with various transition angles, but data for determining the location for maximum SPL are not given. By using the shock location data for a 1-inch model (Ref. 16) and assuming direct scaling, the shock locations for other wind-tunnel models were predicted.

Assuming that the maximum SPL occurs at the position of the shock, maximum SPL location data and shock location data can be treated as identical and can be incorporated into the same graph. Curves of Mach number (at which either the shock or maximum SPL occurs at a particular location) versus the actual distance downstream of a shoulder are given for a variety of model diameters (d), and for three transition angles (θ) in Figure 25 (a-c).

By normalizing the distance data for diameter, nondimensional plots result which collapse reasonably well into a single curve for each transition angle, as shown in Figure 25 (d-f). The collapsing of the data to a single curve indicates x/d scaling of the maximum SPL location data is appropriate, and it lends support to the assumption that the maximum SPL occurs at the shock location.

The correlation of shock location with maximum SPL location is more readily seen in Figure 26, which compares predicted shock location at similar Mach numbers with measured maximum SPL location for a variety of model sizes and transition angles.

A set of design curves for estimating Mach number at which the maximum sound pressure level occurs for a particular transition angle and distance downstream of a shoulder is presented in Figure 27. These curves were derived from Figure 25 (d-f) plus additional shock location data (Ref. 16) for 25- and 30-degree transition angles. As shown by the curves, the location of the maximum SPL changes

rapidly with variations in Mach number (e.g., a 5-percent increase in Mach number results in a doubling of the distance of the maximum SPL from the shoulder).

The effect of angle of attack in determining the location of maximum SPL on the leeward side of a vehicle is shown in Figure 28. Data for plotting these trends were derived from reported results (Ref. 13) for the two-stage model vehicle shown in the sketch. The data are maximum SPL locations averaged for the two diameters. A suggested use for these curves is to indicate the approximate shift in Mach number or x/d to be applied to the curves in Figure 27, which are nominally for 0-degree angle of attack.

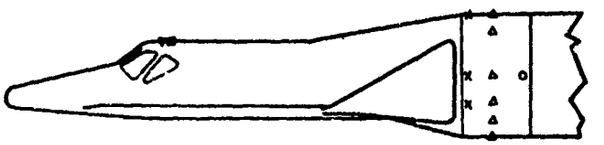

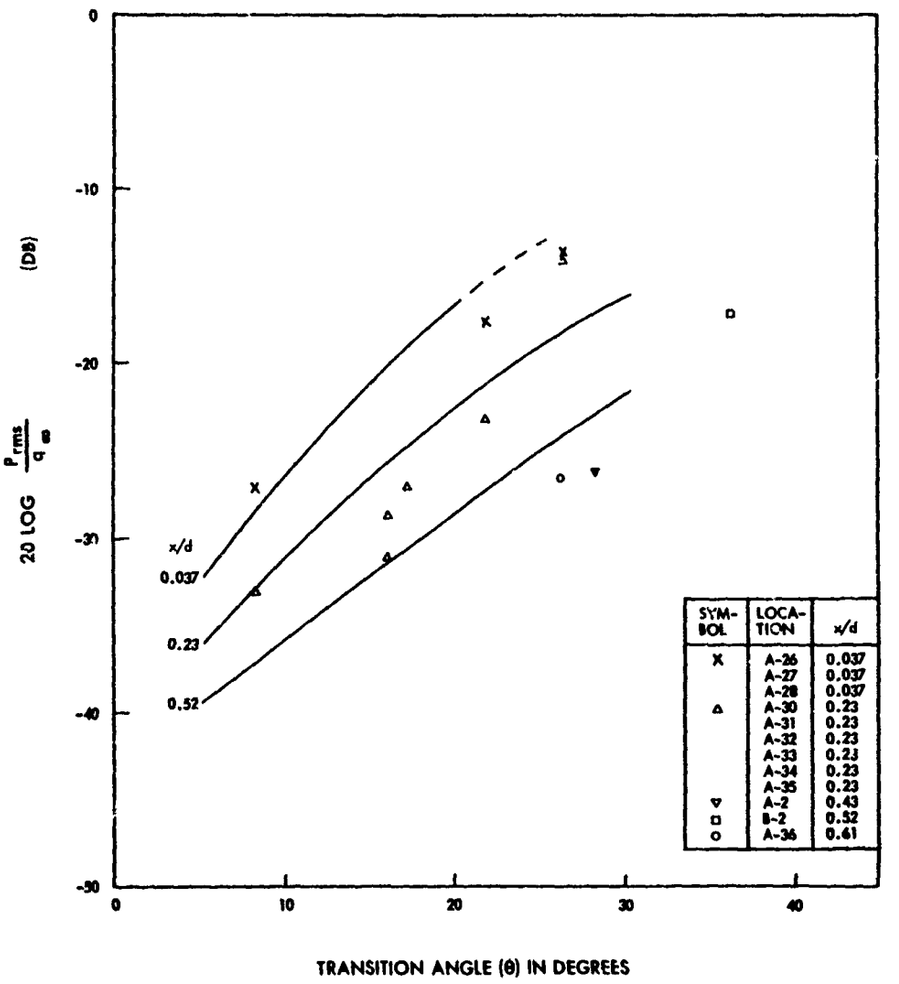

Figure 24: Comparison of Maximum Levels Measured on the X-20 Model With Curves Derived From Design Chart of Figure 23

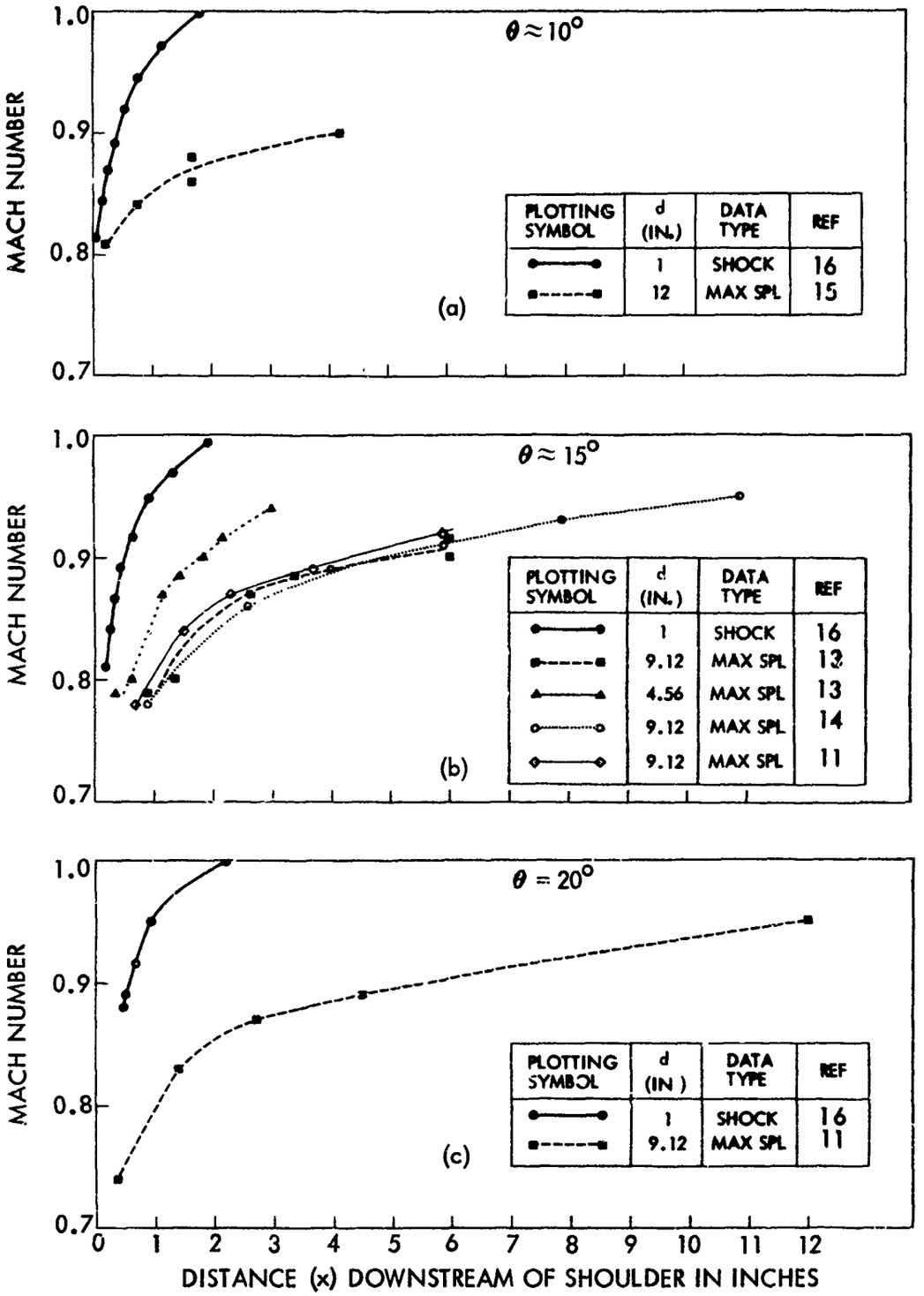

Figure 25 : Mach Number at Which Either Shock or Maximum SPL Occurs as a Function of (1) Actual Distance Downstream of a Shoulder (a-c) and (2) Nondimensional Distance Downstream of a Shoulder (d-f)

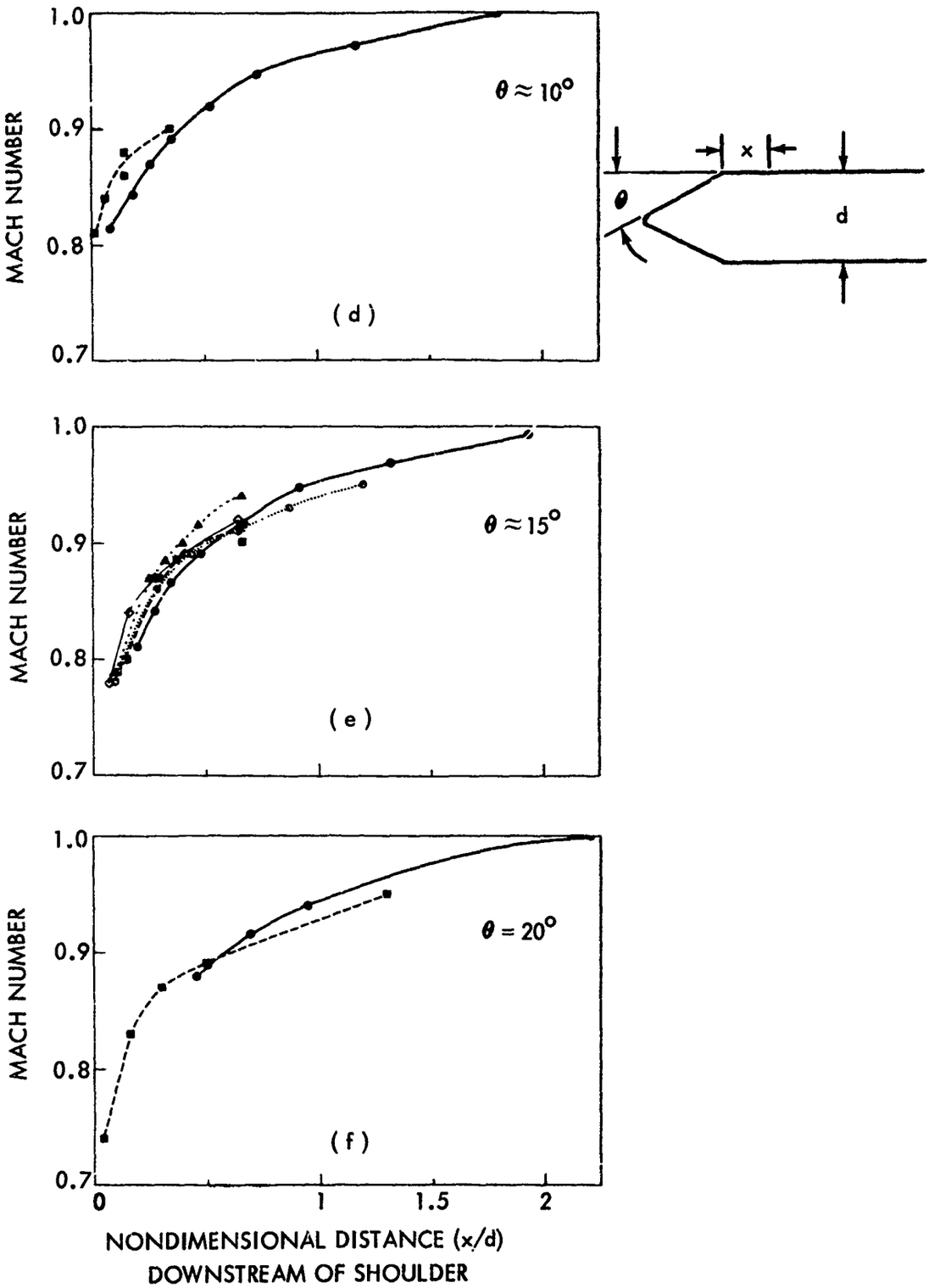

Figure 25 (cont.)

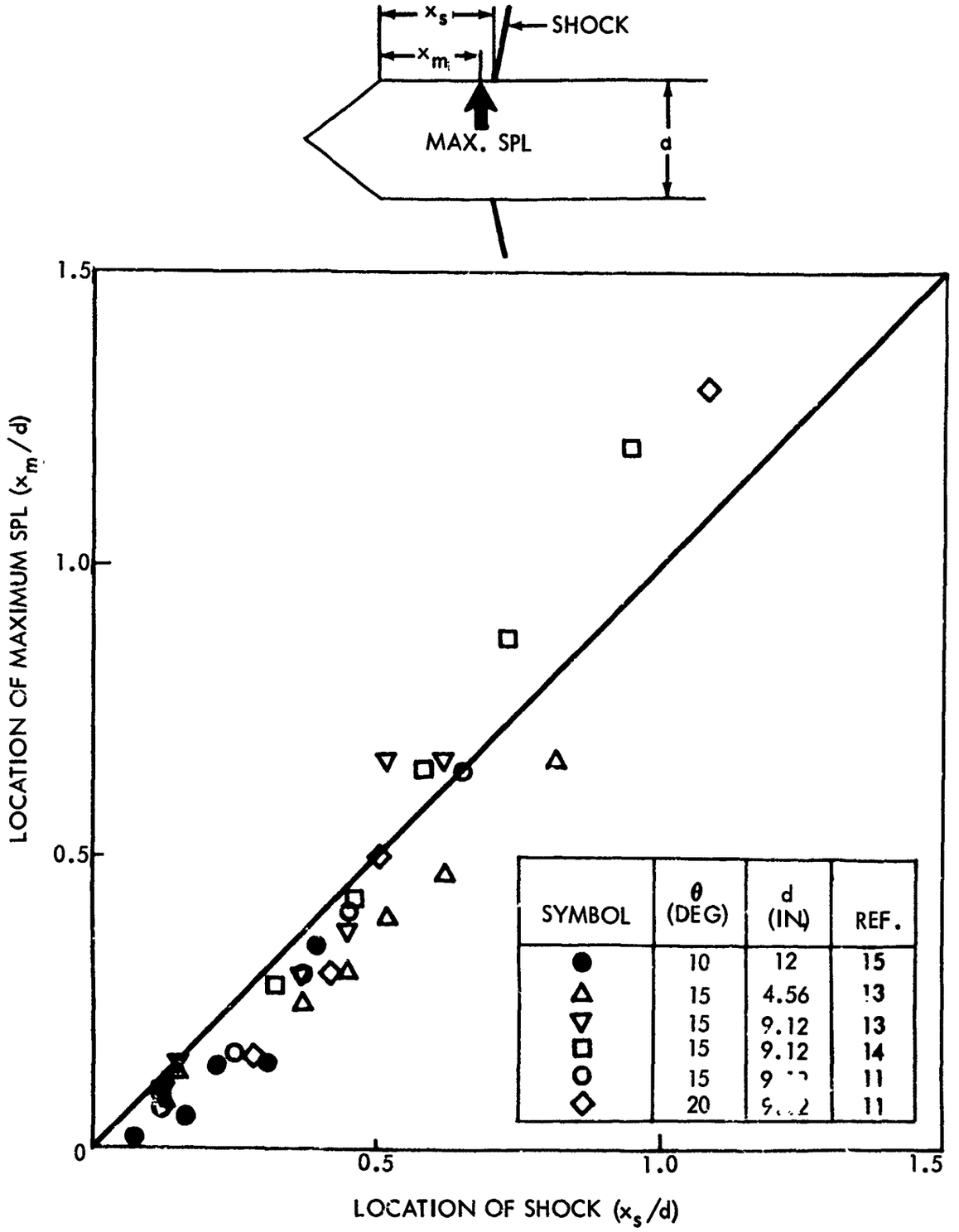

Figure 26 : Correlation of Maximum Sound Pressure Level Location with Shock Location

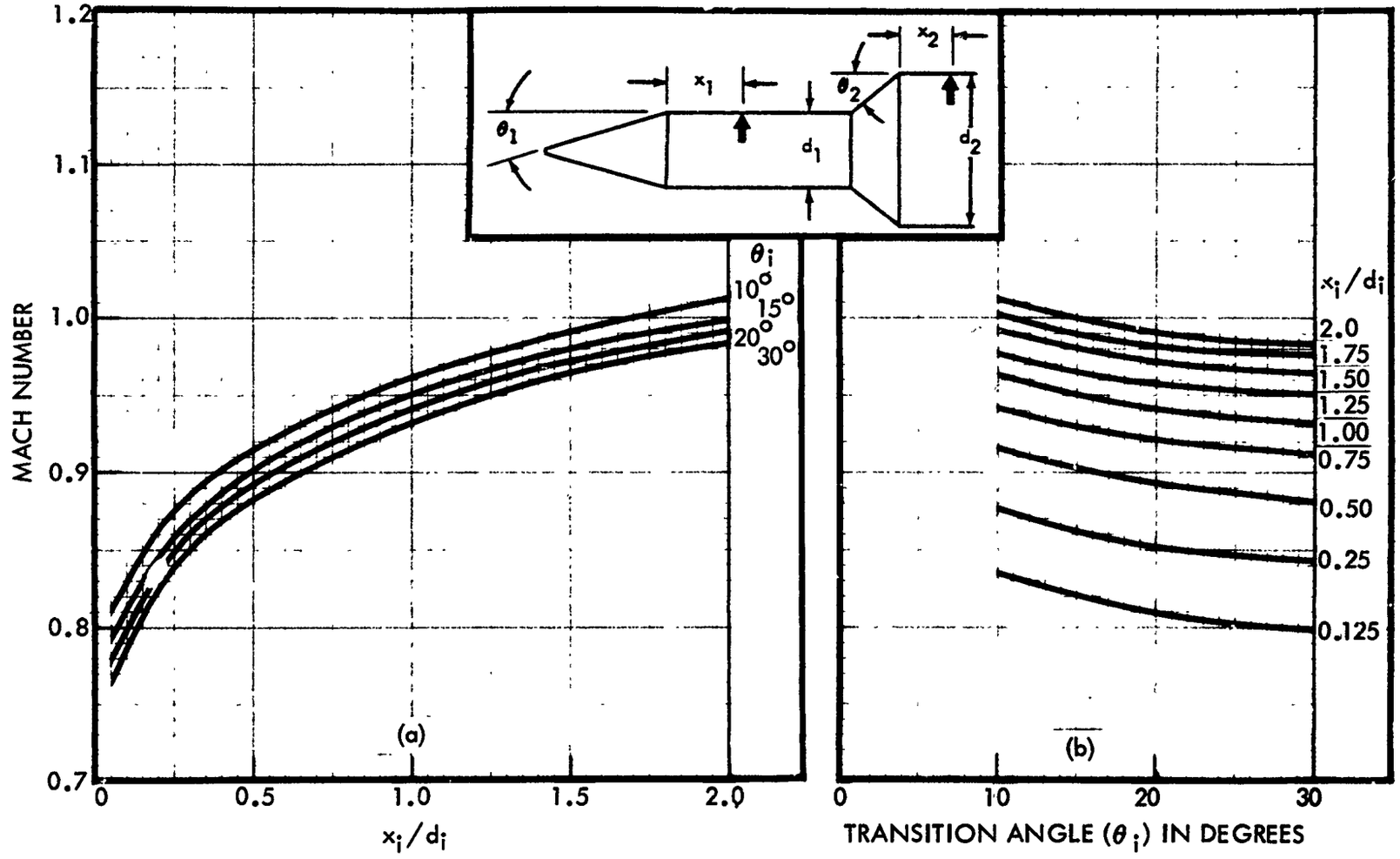

Figure 27: Design Chart for Estimating Mach Number at Which the Maximum Sound Pressure Level Occurs, Given the Transition Angle (θ) and the Nondimensional Distance (x/d) Downstream of a Shoulder.

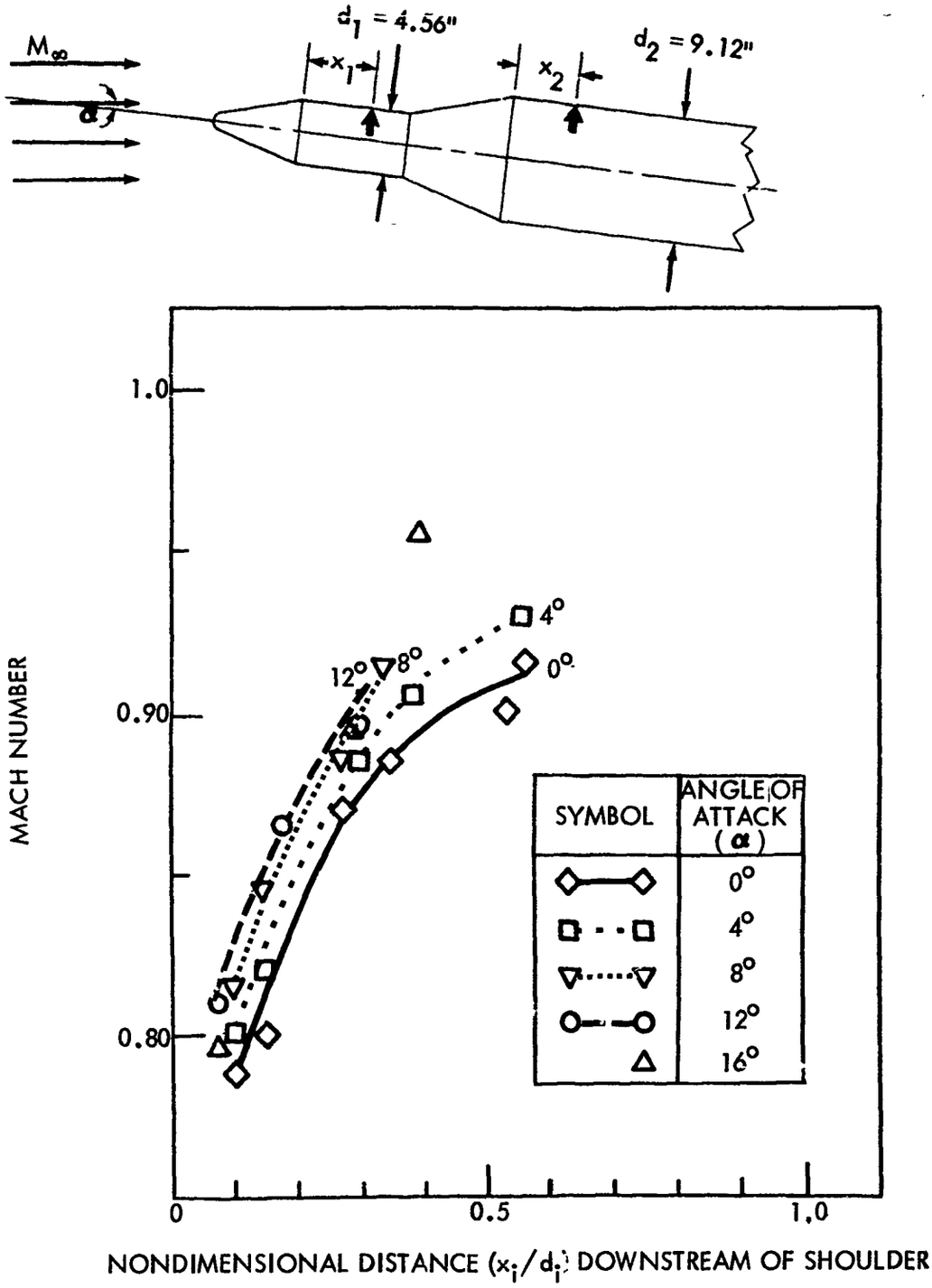

Figure 28: Trends in Location of Maximum Sound Pressure Level and Corresponding Mach Number for Various Angles of Attack (α). Data are for the Leeward Side of a Vehicle with a Transition Angle (θ) of 14.5°.

6.0 CONCLUSIONS AND RECOMMENDATIONS

Highest fluctuating pressure levels occur aft of convex corners, such as transitions to larger vehicle cross sections. These levels increase with steepness of transition angle, and decrease with distance downstream of the shoulder. As the Mach number is increased through the transonic range, the overall SPL at these locations (initially at a high value and peaking at high frequencies) further increases, and the frequency for the peak level typically becomes lower. At a "critical" Mach number, the level drops abruptly and the spectrum peaks at a higher frequency. Future aerodynamic tests should provide for small Mach-number increments (ideally a continuous Mach-number sweep) and closely spaced transducers having a broad frequency response. For an 8-inch-diameter scale model, for example, the transducers should cover a frequency range of 4 to 40,000 cps. This upper frequency limit would correspond to a frequency of approximately 2500 cps for a full-scale vehicle of 120-inch diameter.

The maximum overall rms pressure encountered in transonic flight can be estimated for a given cone-cylinder transition angle (θ), nondimensional distance downstream of shoulder (x/d), and dynamic pressure (q_∞). Similarly, the Mach number at which the maximum sound pressure level will occur can be estimated. Design charts have been derived from the subject study; however, these charts should be validated for a closely controlled set of cone-cylinder models, and should be extended to cover the ranges of transition angles and distance downstream encountered in vehicle design. The results of such a study would also provide a means of predicting spectra associated with the levels obtained. Fluctuating pressure levels near other common configurational features such as protuberances and fairings should also be investigated.

The maximum sound pressure levels occur at the locations predicted for the shock wave, and are attributed to shock/boundary-layer interactions; however, to define adequately the fluctuating pressure source, means for determining associated flow patterns are necessary.

Further recommendations for investigating aerodynamic noise include:

1) Experimental verification of scaling principles;

2) Detailed correlation measurements with closely spaced microphones;

3) Tests with flexible models to investigate the interaction of the aerodynamic pressures and the motion of the structure.

7.0 REFERENCES

1. Sugamele, J., "Pressure Spectra and Space Correlations from Aerodynamic Noise Test," Document D2-80713, The Boeing Company, September 1963.

2. Lockleer, M.D., "X-20/624A Air Vehicle Buffet Test — SPO-203," Test Report T2-2648, The Boeing Company, October 1963.

3. Kistler, A.L., and Chen. W.S., "The Fluctuating Pressure Field in a Supersonic Turbulent Boundary Layer," Journal of Fluid Mechanics, Volume 16, May 1963.

4. Chevalier, H.L., and Robertson, J.E., "Pressure Fluctuations Resulting from an Alternating Flow Separation and Attachment at Transonic Speeds," AEDC-TDR-63-204, Arnold Engineering Development Center, Tullahoma, Tennessee, November 1963.

5. Jones, G.W. Jr., and Foughner, J.T. Jr., "Investigation of Buffet Pressures on Models of Large Manned Launch Vehicle Configurations," NASA TN D-1633, National Aeronautics and Space Administration, Washington, D.C., May 1963.

6. Morgan, W.V., Sutherland, L.C., and Young, K.J., "The Use of Acoustic Scale Models for Investigating Near Field Noise of Jet and Rocket Engines," WADD Technical Report 61-178, Wright Air Development Division, Wright-Patterson AFB, Ohio, April 1961.

7. Richards, E.J., Bull, M.K., and Willis, J.L., "Boundary Layer Noise Research in the U.S.A. and Canada; a Critical Review," U.S.A.A. Report No. 131, University of Southampton, February 1960.

8. Rainey, A.G., "Progress on the Launch Vehicle Buffeting Problem," AIAA Publication CP-8, Fifth Annual AIAA Structures and Materials Conference, April 1-3, 1964.

9. Lee, Y.W., Statistical Theory of Communication, John Wiley & Sons, Inc., New York, 1960.

10. Bendat, J.S., Principles and Applications of Random Noise Theory, John Wiley & Sons, Inc., New York, 1958.

11. Coe, C.F., and Kaskey, A.J., "The Effects of Nose Bluntness on the Pressure Fluctuations Measured on 15° and 20° Cone-Cylinders at Transonic Speeds," NASA TM X-779, National Aeronautics and Space Administration, Washington, D.C., January 1963.

12. Unpublished data from a Boeing wind tunnel test.

13. Coe, C.F., "The Effects of Some Variations in Launch-Vehicle Nose Shape on Steady and Fluctuating Pressures at Transonic Speeds," NASA TM X-646, National Aeronautics and Space Administration, Washington, D.C., March 1962.

14. Coe, C.F., "Steady and Fluctuating Pressures at Transonic Speeds on Two Space-Vehicle Payload Shapes," NASA TM X-503, National Aeronautics and Space Administration, Washington, D.C., March 1961.

15. Coe, C.F., and Nute, J.B., "Steady and Fluctuating Pressures at Transonic Speeds on Hammerhead Launch Vehicles," NASA TM X-778, National Aeronautics and Space Administration, Washington, D.C., December 1962.

16. Chevalier, H.L., and Robertson, J.E., "Characteristics of Steady-State Pressures on the Cylindrical Portion of Cone-Cylinder Bodies at Transonic Speeds," AEDC-TDR-63-104, Arnold Engineering Development Center, Tullahoma, Tennessee, August 1963.

UNCLASSIFIED

Security Classification

DOCUMENT CONTROL DATA - R&D

(Security classification of title, body of abstract and indexing annotation must be entered when the overall report is classified)

1 ORIGINATING ACTIVITY (Corporate author) The Boeing Company Aerospace Division PO Box 3707 Seattle Wash 98124	2a. REPORT SECURITY CLASSIFICATION UNCLASSIFIED 2b. GROUP N/A

3. REPORT TITLE

Aerodynamic Noise Tests on X-20 Scale Models
Vol II Summary and Analysis Report

4. DESCRIPTIVE NOTES (Type of report and inclusive dates)

Final Report October 1961 to August 1965

5 AUTHOR(S) (Last name, first name, initial)

Wiley, David R.
Seidl, Michael G.

6 REPORT DATE	7a. TOTAL NO. OF PAGES	7b. NO. OF REFS
November 1965	58	16

8a. CONTRACT OR GRANT NO.	9a. ORIGINATOR'S REPORT NUMBER(S)
Reinstated Documentation Sub-Item 8-46 Contract AF 33(657)-7132 b. PROJECT NO. 1471 c. Task 147102 d.	AFFDL-TR-65-192, Volume II 9b. OTHER REPORT NO(S) (Any other numbers that may be assigned this report)

10. AVAILABILITY/LIMITATION NOTICES Qualified requesters may obtain cys of this rpt fr DDC. This document is subject to special export controls & each transmittal to foreign governments or foreign nationals may be made only with prior approval of AF Flight Dynamics Laboratory (FDD).

11. SUPPLEMENTARY NOTES	12. SPONSORING MILITARY ACTIVITY
	Air Force Flight Dynamics Laboratory Wright-Patterson AFB, Ohio 45433

13 ABSTRACT

Summaries of fluctuating pressure data presented in Volume I for 1/15th-scale X-20 models are made and discussed. Particular emphasis is given to the high overall rms pressures measured aft of convex corners during transonic test conditions. Additional information relating to these pressures is presented in the form of pressure histories, peak-amplitude distributions, and power spectral densities. Fluctuating-pressure data and space correlation measurements for three closely spaced microphones are presented, illustrating the local nature of the high-level pressures. Analyses of trends for the maximum overall rms pressure levels for the X-20 tests and other wind-tunnel tests are made. Design charts are developed for predicting maximum levels aft of cone-cylinder transition sections as functions of transition angle and distance downstream of the transition shoulder. Recommendations are made regarding future aerodynamic noise experimental programs.

DD FORM 1 JAN 64 1473

UNCLASSIFIED

Security Classification

14. KEY WORDS	LINK A		LINK B		LINK C	
	ROLE	WT	ROLE	WT	ROLE	WT
Dynasoar Aerodynamic Noise Acoustics Pressure Fluctuations Separated Flow Oscillating Shocks Boundary Layer						

INSTRUCTIONS

1. ORIGINATING ACTIVITY: Enter the name and address of the contractor, subcontractor, grantee, Department of Defense activity or other organization *(corporate author)* issuing the report.

2a. REPORT SECURITY CLASSIFICATION: Enter the overall security classification of the report. Indicate whether "Restricted Data" is included. Marking is to be in accordance with appropriate security regulations.

2b. GROUP: Automatic downgrading is specified in DoD Directive 5200.10 and Armed Forces Industrial Manual. Enter the group number. Also, when applicable, show that optional markings have been used for Group 3 and Group 4 as authorized.

3. REPORT TITLE: Enter the complete report title in all capital letters. Titles in all cases should be unclassified. If a meaningful title cannot be selected without classification, show title classification in all capitals in parenthesis immediately following the title.

4. DESCRIPTIVE NOTES: If appropriate, enter the type of report, e.g., interim, progress, summary, annual, or final. Give the inclusive dates when a specific reporting period is covered.

5. AUTHOR(S): Enter the name(s) of author(s) as shown on or in the report. Enter last name, first name, middle initial. If military, show rank and branch of service. The name of the principal author is an absolute minimum requirement.

6. REPORT DATE: Enter the date of the report as day, month, year; or month, year. If more than one date appears on the report, use date of publication.

7a. TOTAL NUMBER OF PAGES: The total page count should follow normal pagination procedures, i.e., enter the number of pages containing information.

7b. NUMBER OF REFERENCES: Enter the total number of references cited in the report.

8a. CONTRACT OR GRANT NUMBER: If appropriate, enter the applicable number of the contract or grant under which the report was written.

8b, 8c, & 8d. PROJECT NUMBER: Enter the appropriate military department identification, such as project number, subproject number, system numbers, task number, etc.

9a. ORIGINATOR'S REPORT NUMBER(S): Enter the official report number by which the document will be identified and controlled by the originating activity. This number must be unique to this report.

9b. OTHER REPORT NUMBER(S): If the report has been assigned any other report numbers *(either by the originator or by the sponsor)*, also enter this number(s).

10. AVAILABILITY/LIMITATION NOTICES: Enter any limitations on further dissemination of the report, other than those imposed by security classification, using standard statements such as:

(1) "Qualified requesters may obtain copies of this report from DDC."

(2) "Foreign announcement and dissemination of this report by DDC is not authorized."

(3) "U. S. Government agencies may obtain copies of this report directly from DDC. Other qualified DDC users shall request through _____."

(4) "U. S. military agencies may obtain copies of this report directly from DDC. Other qualified users shall request through _____."

(5) "All distribution of this report is controlled. Qualified DDC users shall request through _____."

If the report has been furnished to the Office of Technical Services, Department of Commerce, for sale to the public, indicate this fact and enter the price, if known.

11. SUPPLEMENTARY NOTES: Use for additional explanatory notes.

12. SPONSORING MILITARY ACTIVITY: Enter the name of the departmental project office or laboratory sponsoring *(paying for)* the research and development. Include address.

13. ABSTRACT: Enter an abstract giving a brief and factual summary of the document indicative of the report, even though it may also appear elsewhere in the body of the technical report. If additional space is required, a continuation sheet shall be attached.

It is highly desirable that the abstract of classified reports be unclassified. Each paragraph of the abstract shall end with an indication of the military security classification of the information in the paragraph, represented as *(TS), (S), (C), or (U)*

There is no limitation on the length of the abstract. However, the suggested length is from 150 to 225 words.

14. KEY WORDS: Key words are technically meaningful terms or short phrases that characterize a report and may be used as index entries for cataloging the report. Key words must be selected so that no security classification is required. Identifiers, such as equipment model designation, trade name, military project code name, geographic location, may be used as key words but will be followed by an indication of technical context. The assignment of links, rules, and weights is optional.